X-ray physics relevant for MA-XRF

Andreas - Germanos Karydas

Institute of Nuclear and Particle Physics
National Centre for Scientific Research “Demokritos”
Aghia Paraskevi, Athens, Greece

karydas@inp.demokritos.gr

Outline

- Fundamental interactions: X-rays and matter
- Qualitative and Quantitative XRF Analysis:
  Basic principles
- Second order phenomena in Q-XRF and MAXRF
- XRF Instrumentation with relevance to imaging:
  - X-rays sources
  - X-ray Optics
  - X-ray detectors
- MAXRF spectrometers: Figures of merit
- Conclusions

(ED) XRF principle of operation

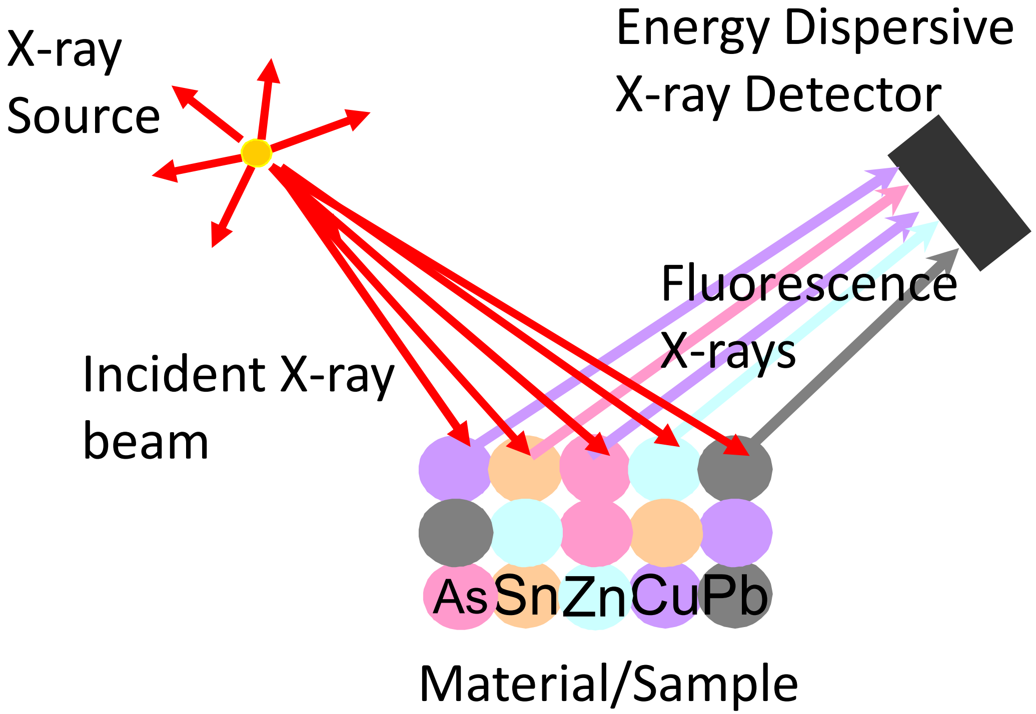

XRF is an analytical technique based on the **spectroscopy** of the **fluorescence** ("characteristic") **x-ray** radiation emitted from the material/sample when it is irradiated **by x-rays**.

- **Spectroscopy** – measurement of a signal (number of x-rays) versus energy; formation of a **spectrum**
- **Fluorescence/characteristic x-ray radiation** emitted from **the elements** contained in the material/sample analyzed
- **X-rays** – used for both excitation and detection

X-rays interactions with matter

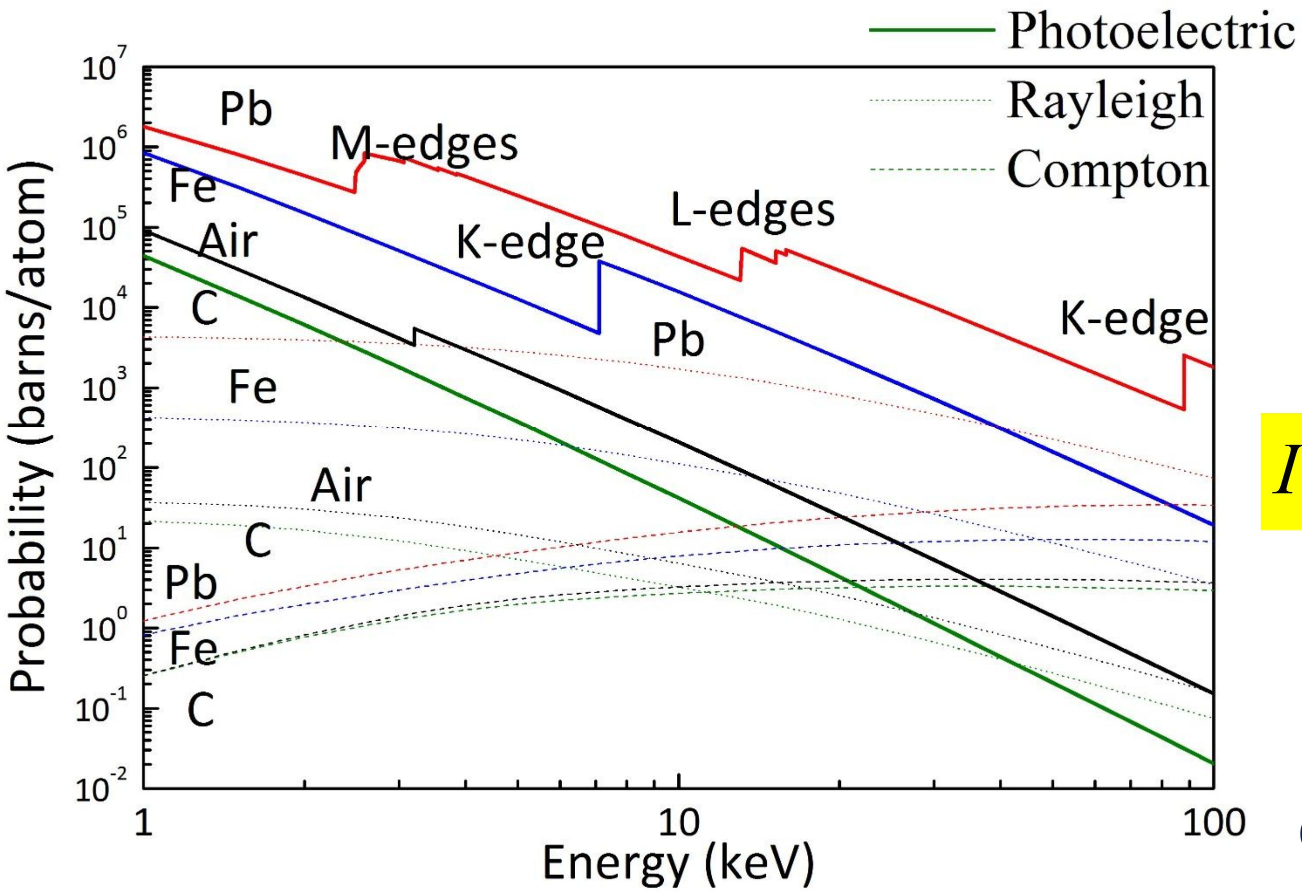

Beer-Lambert law

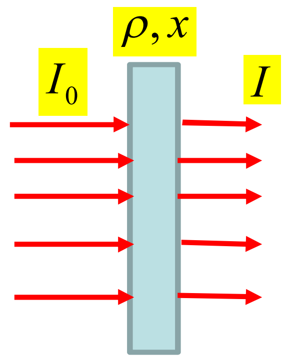

$$I = I_0 \cdot e^{-(\tau+\sigma_R+\sigma_C)\cdot\rho\cdot x}$$

Ratio photo./scat.

≈ **1000 - 10000**

Photoelectric is the dominant process

X-ray Scattering Interactions with atoms

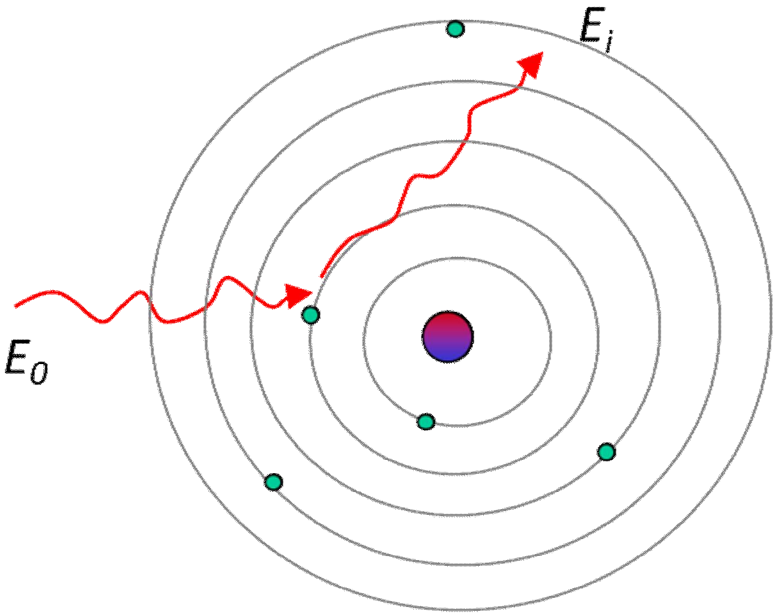

E_0>>Binding Energy

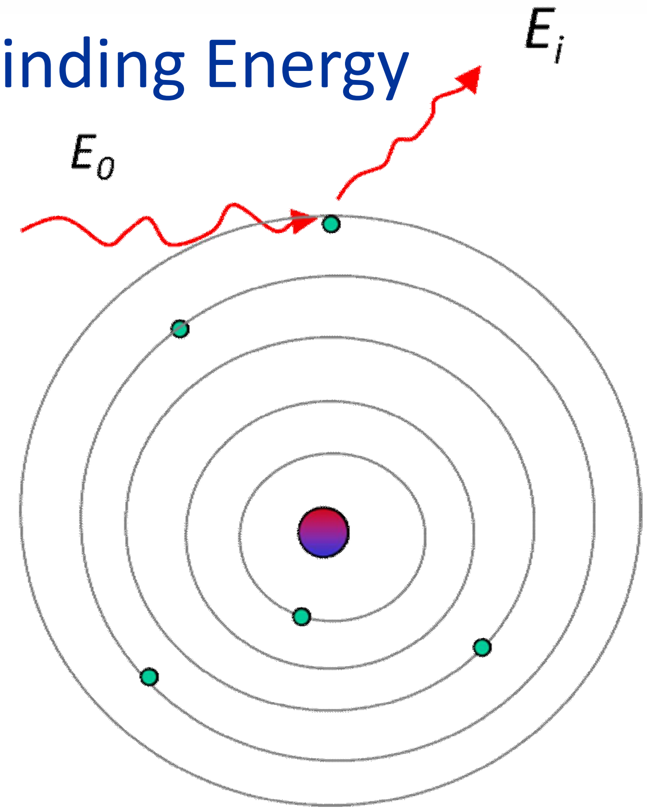

***E_i=E_0* : Coherent (Rayleigh),** it occurs mostly with inner atomic electrons

E_i < E_0: Incoherent (Compton), it occurs mostly with outer, less bound electrons

X-ray scattering with matter (1)

1) Rayleigh/Elastic/Coherent scattering

Compound	(%)
Al_2O_3	16
SiO_2	57
CaO	13
Fe_2O_3	14

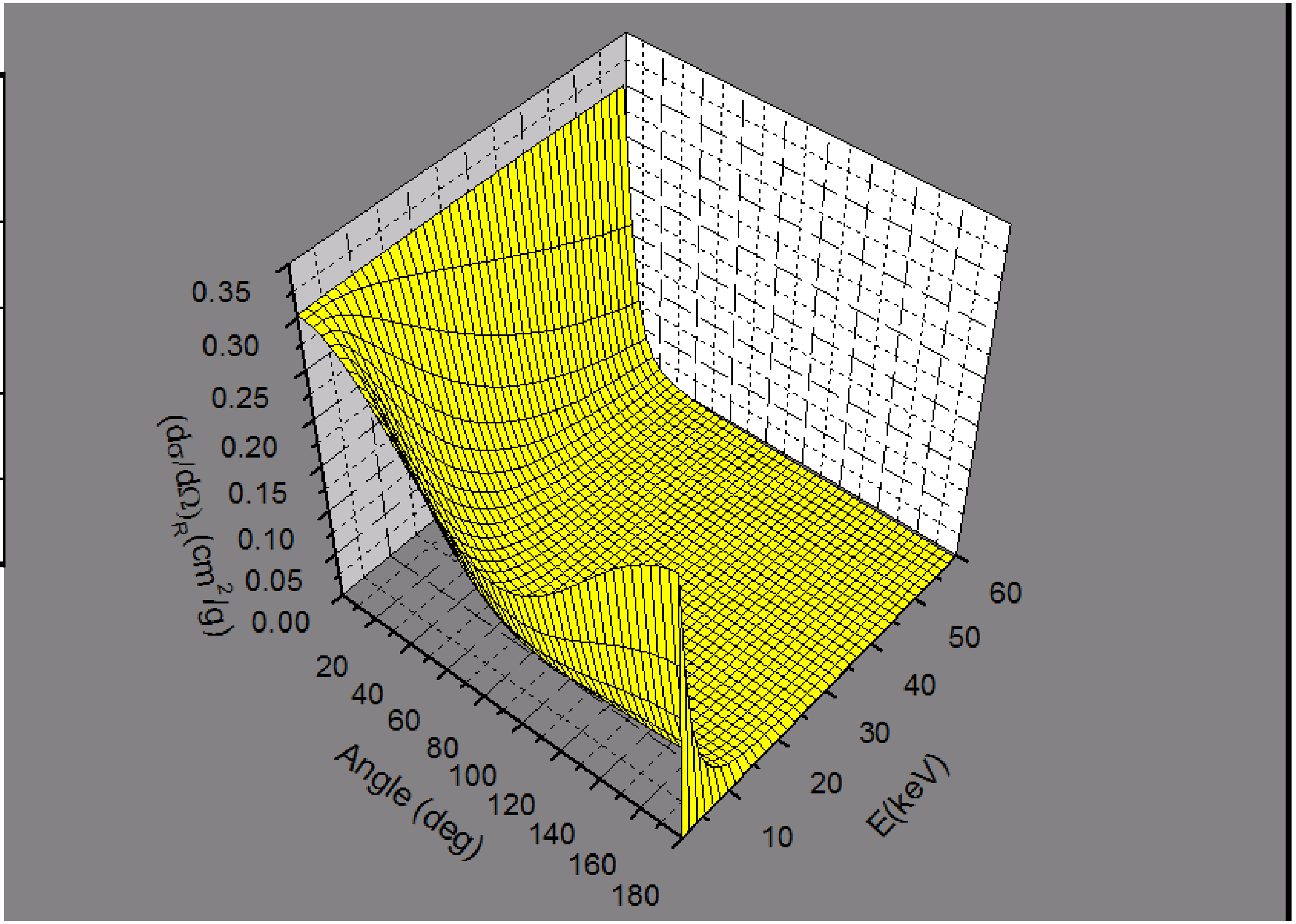

Probability: Increases with 3rd-4th power of Z

X-ray scattering with matter (1)

1) Rayleigh/Elastic/Coherent scattering

Compound	(%)
Al_2O_3	16
SiO_2	57
CaO	13
Fe_2O_3	14

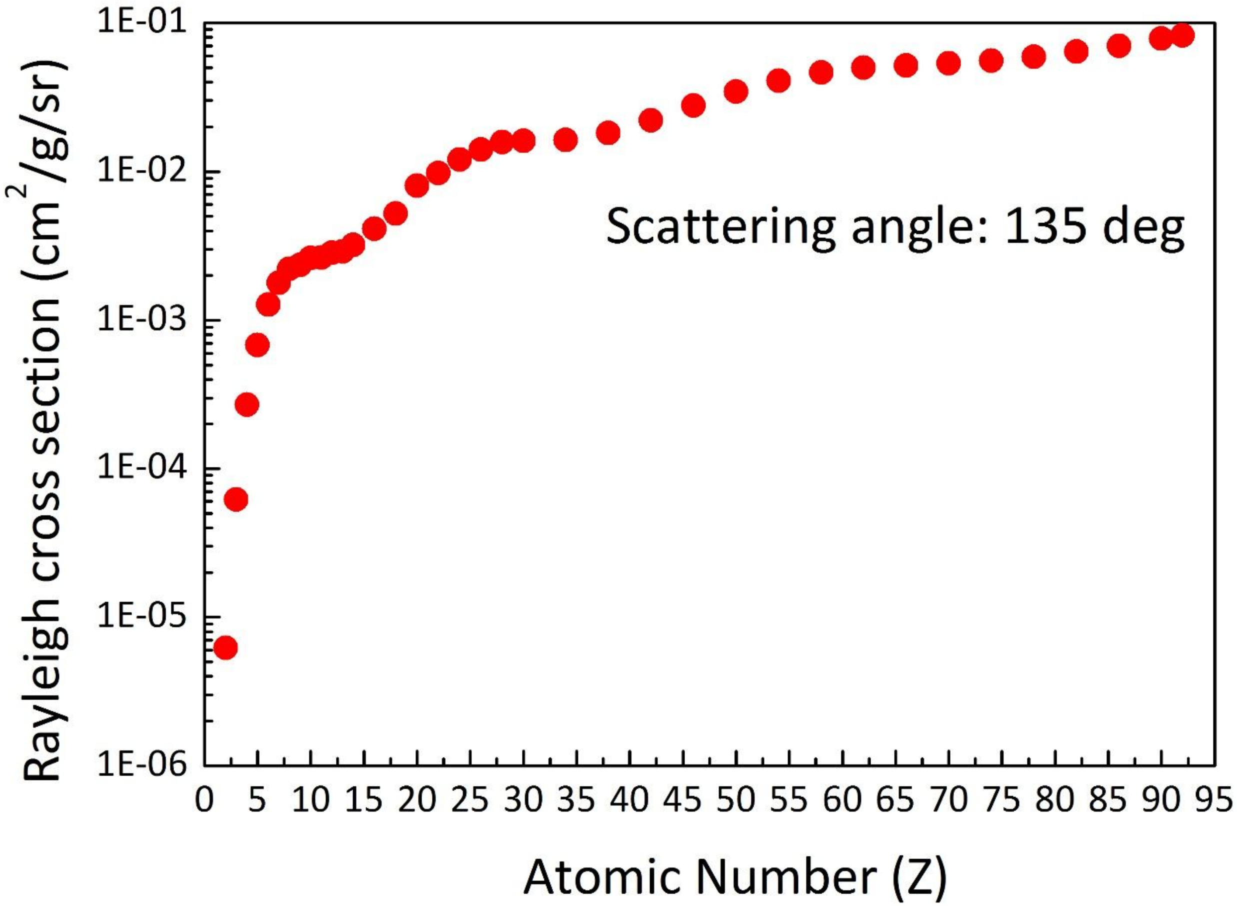

X-ray scattering with matter (2)

Compton/Inelastic/Incoherent scattering

Compound	(%)
Al_2O_3	16
SiO_2	57
CaO	13
Fe_2O_3	14

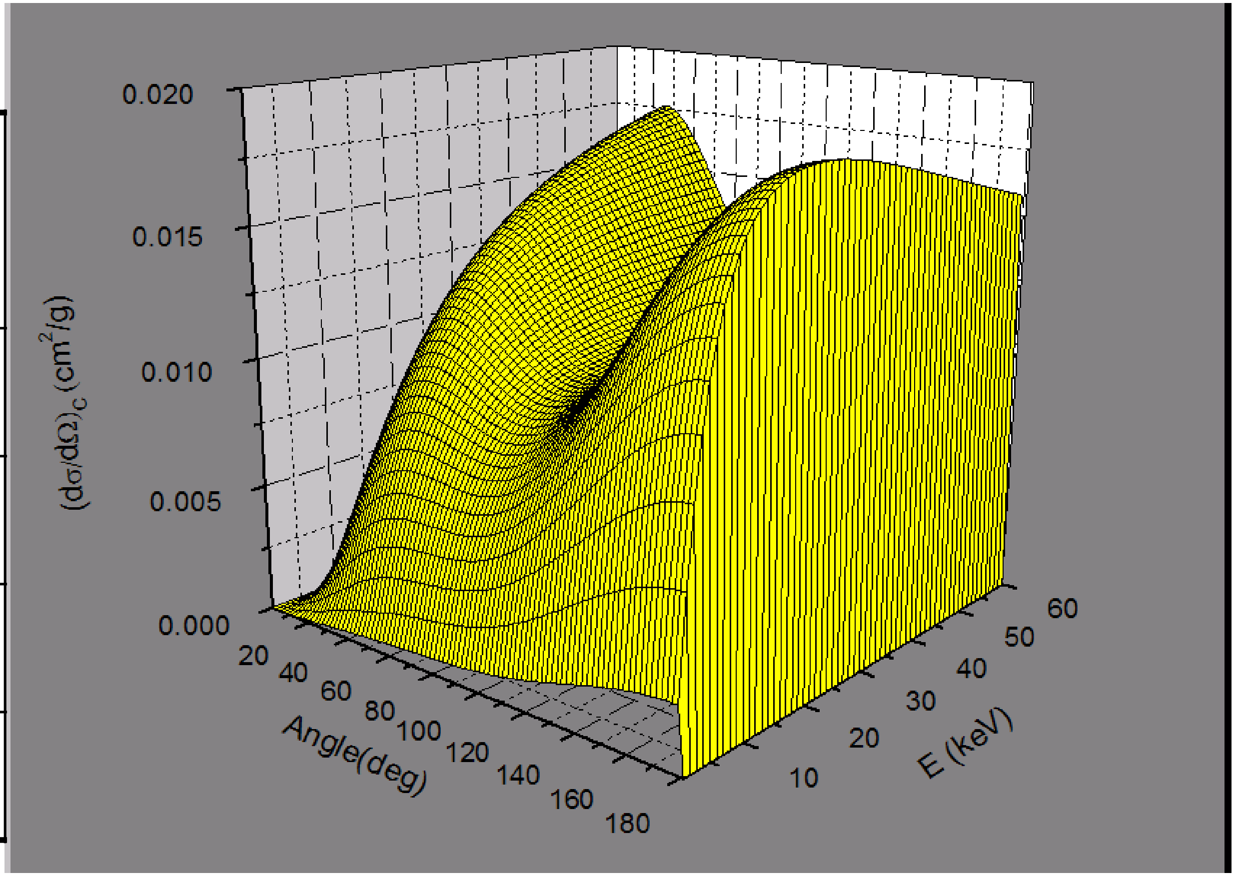

E_i < E_0: Incoherent (Compton), mostly with outer, less bound electrons

X-ray scattering with matter (2)

Compton/Inelastic/Incoherent scattering

Compound	(%)
Al_2O_3	16
SiO_2	57
CaO	13
Fe_2O_3	14

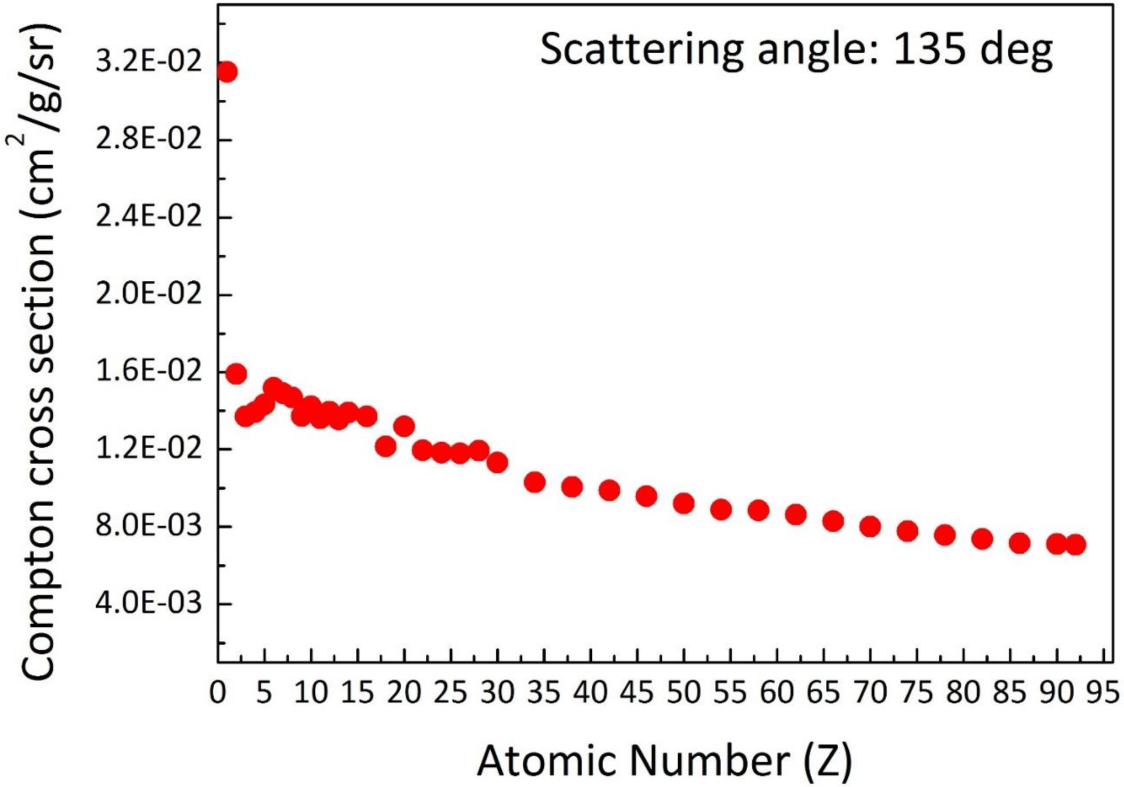

$E_i < E_0$: Incoherent (Compton), mostly with outer, less bound electrons

Photoelectric cross sections: Probabilities

K-shell Photoelectric cross sections

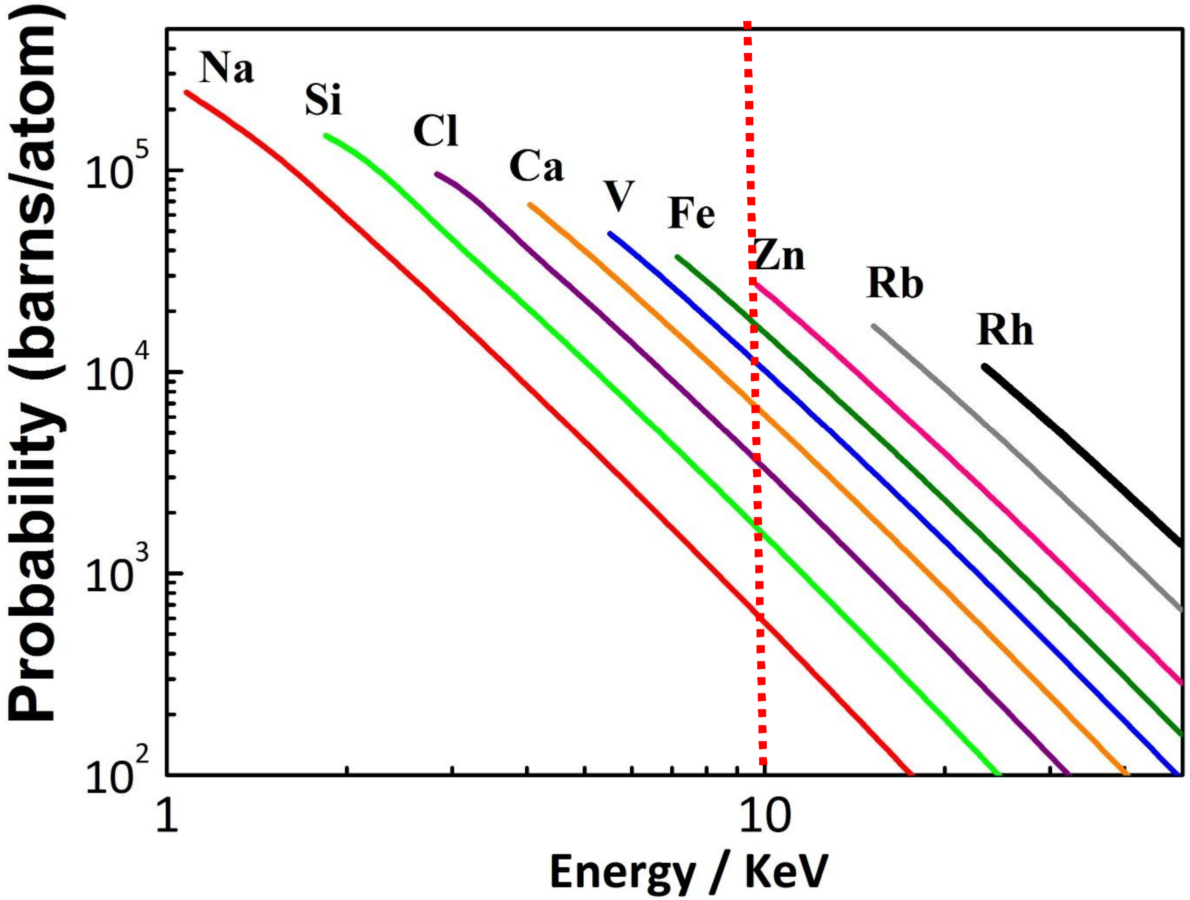

Photoelectric cross section:

$$\tau \sim E^{-3.5}$$

$$\tau \sim Z^{3\ to\ 4}$$

De-excitation: Fluorescence/Auger yield

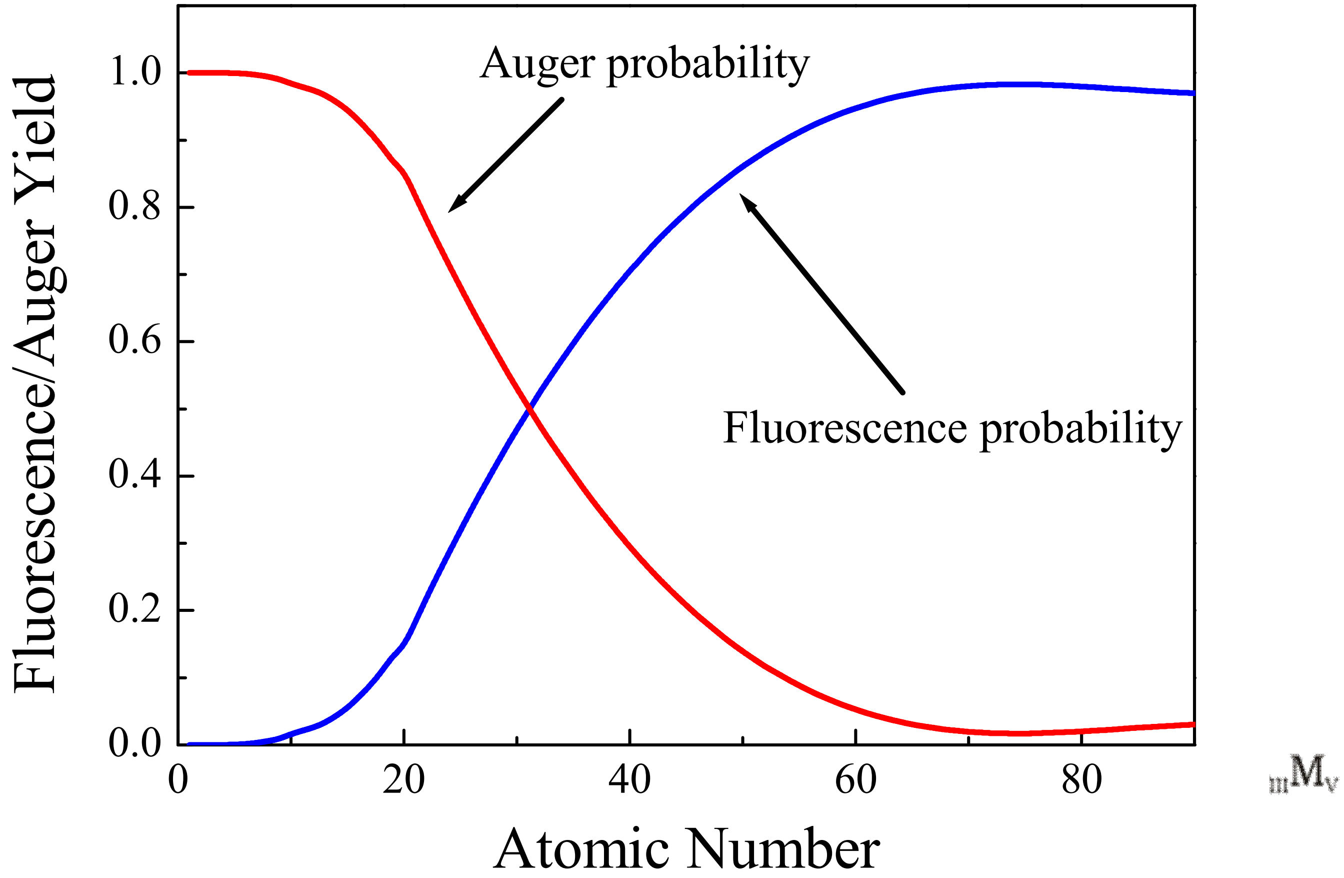

Fluorescence Yield: Very small for low Z elements!!!

Only 5 holes over 100 are filled through the emission of characteristic radiation for Silicon (Z=14) atoms

Emission of element ‘characteristic’ x-rays

The emission of characteristic X-ray lines follows allowed electronic transitions between specific subshells

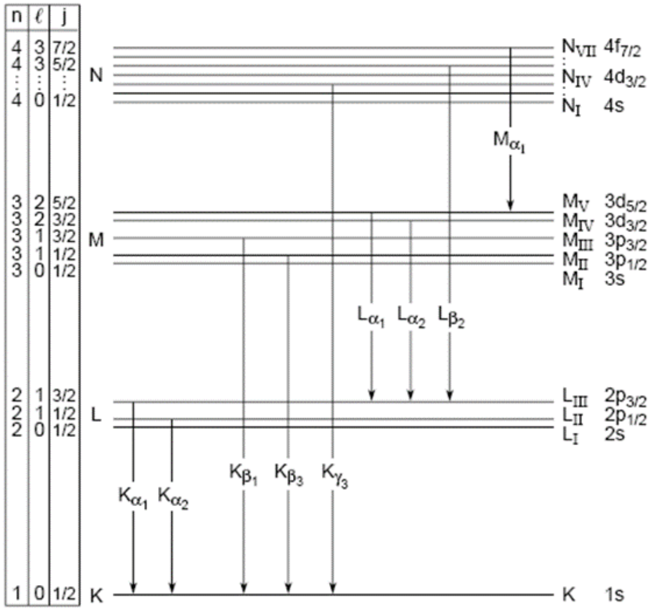

Siegbahn/IUPAC notation:

Kα: K-L2+K-L3

Kβ: K-M2+K-M3

Lα: L3-M4+L3-M5

Lβ$_1$: L2-M4
Lβ$_2$: L3-N5

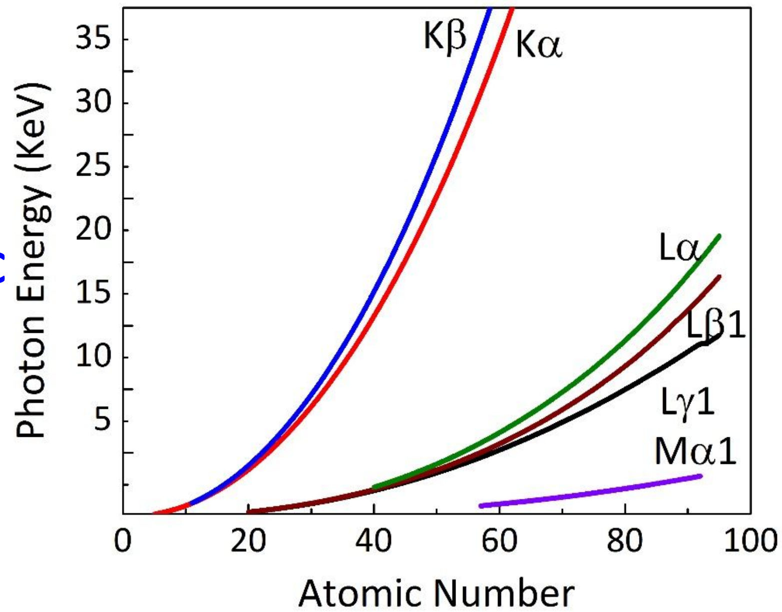

X-ray spectroscopy within the energy range 1-30keV offers in principle the possibility to detect all the periodic table elements through their K, L or even M series of characteristic X-ray lines

Moseley law: $E_{ij} = k_{ij} \cdot (Z - \sigma_i)^2$

L_{III} to K shell: $E_{K\alpha 1} = U_K - U_{LIII}$

Unique set of emission energies for each element

Working principle: X-Ray Fluorescence Analysis

Working principle:

1) Photo-Ionization of **atomic bound electrons** (K, L, M) /**Photoelectric absorption**

2) Electronic transition and emission of element **'characteristic' fluorescence** radiation

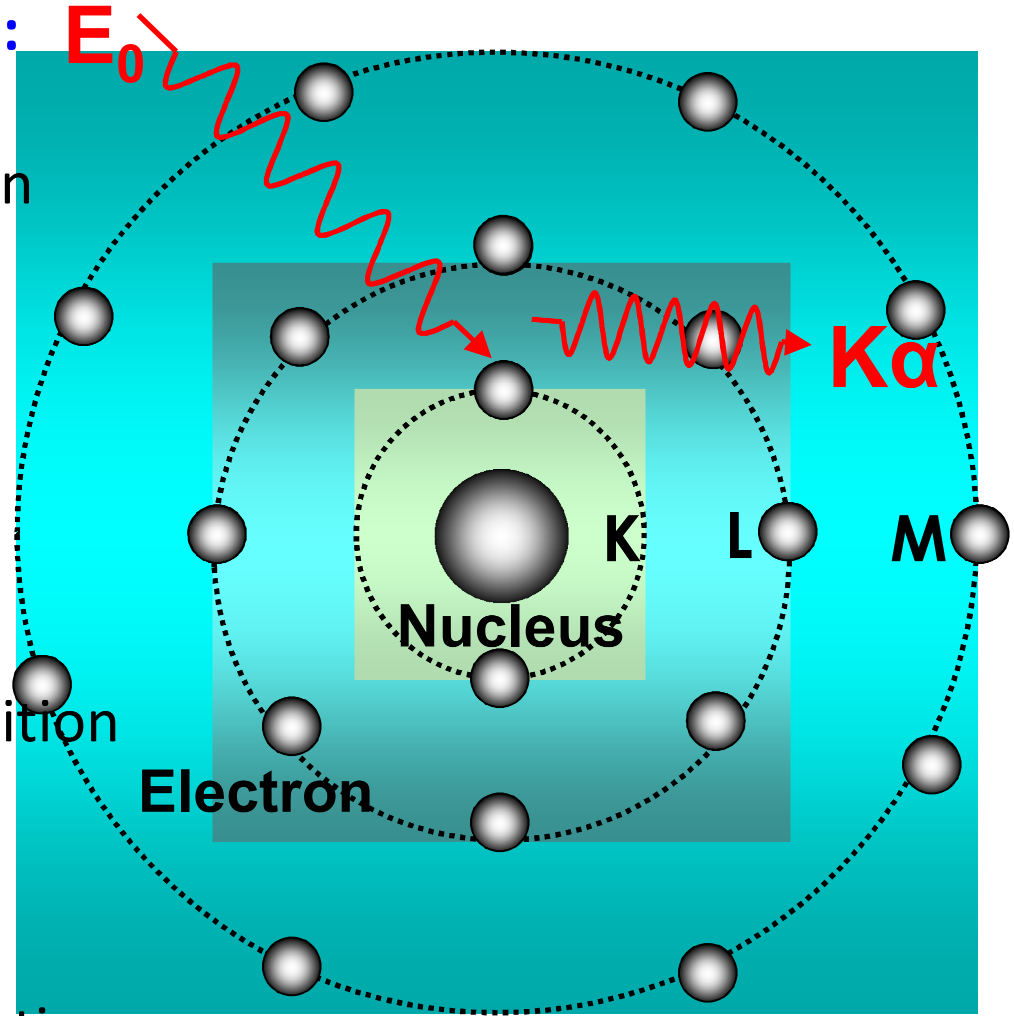

Incident photon Energy E_0 should be adequate to ionize the atomic bound electrons >= Inner shell binding energy

Fluorescence cross sections: Selective excitation

XRF K-shell fluorescence cross section $\sigma_{KX}(E_o)$

$$\sigma_{KX}(E_o) = \tau_K(E_o) \cdot \omega_K \cdot F_{KX}$$

Transition probability for Kα emission

K-shell photoelectric cross section

K-shell fluorescence yield

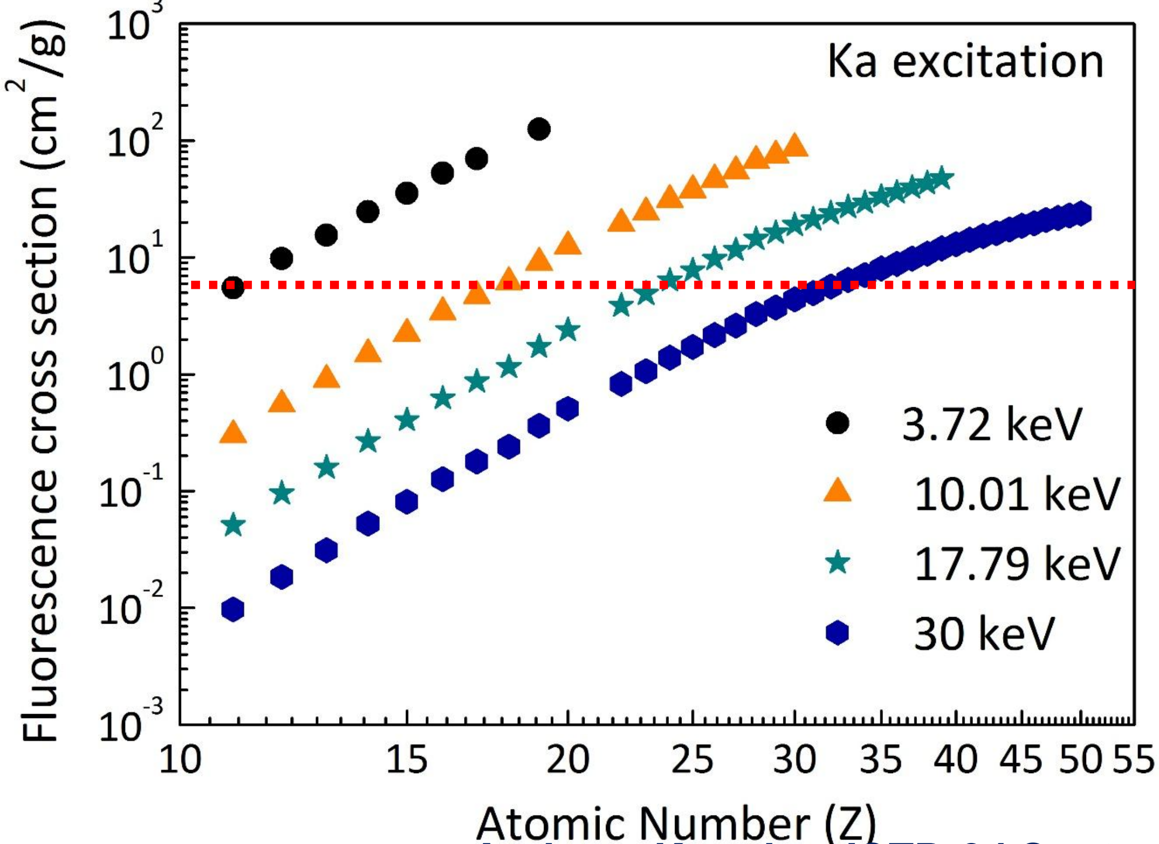

Optimizing the energy of the exciting beam for maximizing the produced characteristic X-ray intensity

Primary Fluorescence intensity: Assumptions

Spectrochimica Acta, 1955, Vol 7, pp 283 to 306. Pergamon Press Ltd., London

JAPANESE JOURNAL OF APPLIED PHYSICS VOL. 5, NO. 10, OCTOBER, 196

Theoretical Calculation of Fluorescent X-Ray Intensities in Fluorescent X-Ray Spectrochemical Analysis.

Toshio SHIRAIWA and Nobukatsu FUJINO
Physics Section, Central Research Laboratories, Sumitomo Metal Industries, Amagasaki, Hyogo.

(Received April 15, 1966)

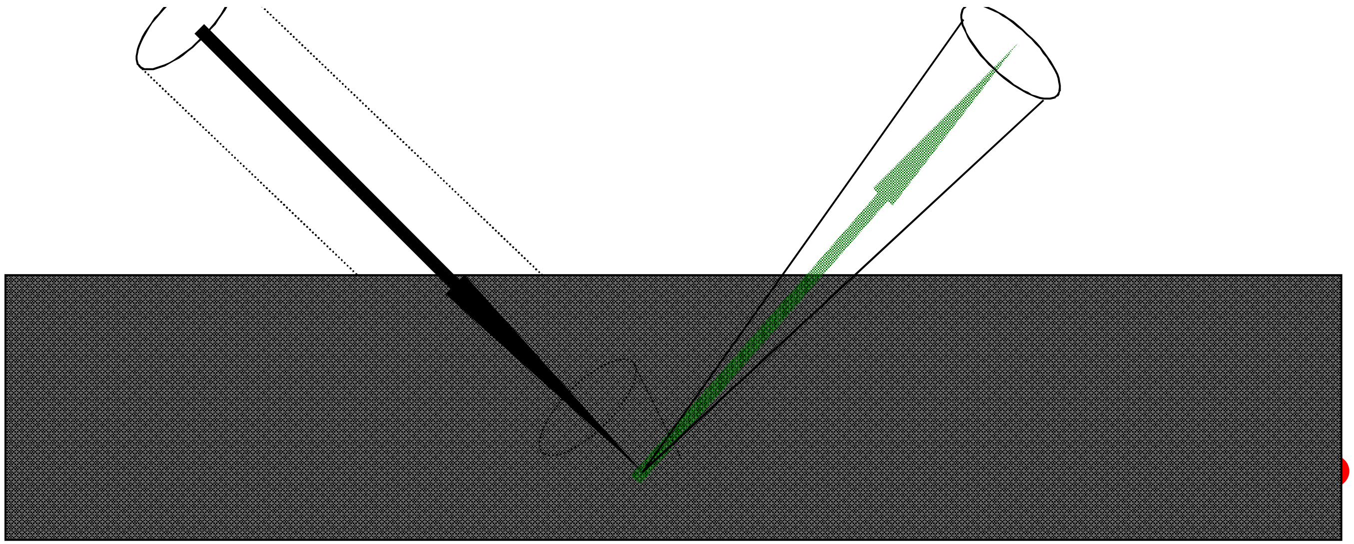

Primary XRF intensity

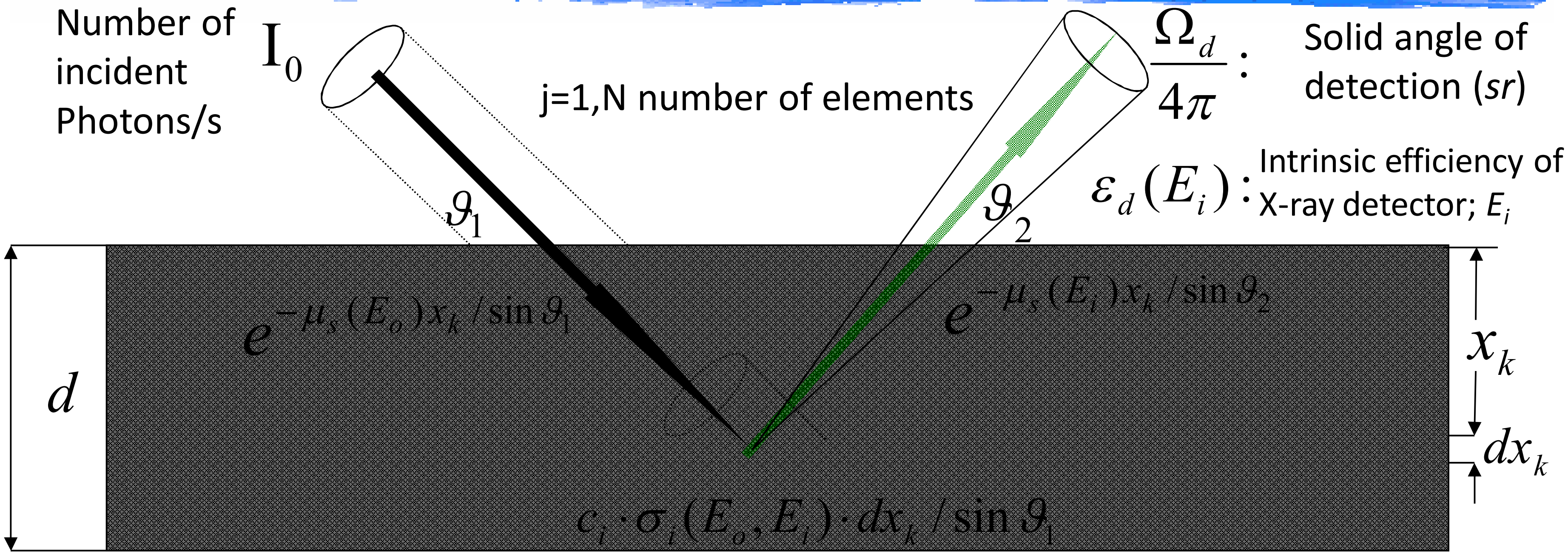

(Concentration of *i* element) X (Fluorescence cross section; cm^2/g) X (areal density; g/cm^2)

$\mu_s(E_o)$: Sample mass attenuation coefficient for energy Eo $\equiv \sum_{j=1,N} c_j \mu_j(E_o)$

$$dI_i(E_i) = I_o \cdot e^{-\mu_s(E_o)\cdot x_k/\sin\vartheta_1} c_i \cdot \sigma_i(E_o, E_i) \cdot \frac{dx_k}{\sin\vartheta_1} \cdot e^{-\mu_s(E_i)\cdot x_k/\sin\vartheta_2} \frac{\Omega_d}{4\cdot\pi} \cdot \varepsilon_d(E_i)$$

$$\mu_T(E_o, E_i) \equiv \mu_s(E_o)/\sin\vartheta_1 + \mu_s(E_i)/\sin\vartheta_2$$

Primary XRF intensity: Approximations

$$I_i(E_i) = c_i \cdot \frac{1}{\sin \vartheta_1} \cdot \frac{\Omega_d}{4 \cdot \pi} \cdot \varepsilon_d(E_i) \int_{U_{Xi}}^{Eo} I(E) \cdot \sigma_i(E, E_i) \cdot \frac{1 - e^{-\mu_T(E,E_i)\cdot d}}{\mu_T(E, E_i)} \cdot dE$$

Sensitivity $S_i(E_o, E_i)$

$\mu_T(E_o, E_i) \cdot d \gg 1$ $$I_i(E_i) = S_i(E_o, E_i) \cdot c_i \cdot \frac{1}{\mu_T(E_o, E_i)}$$ **Thick target approximation**

$\mu_T(E_o, E_i) \cdot d \ll 1$ $$I_i(E_i) = S_i(E_o, E_i) \cdot c_i \cdot d$$ **Thin target approximation**

- **Sensitivity calibration:** certified pure element/compound targets
- **Solid angle/Intensity calibration:** Energy distribution, detector efficiency known, well certified pure element/compound targets
- **Standard-less XRFA:** Calibrated apertures, distances, detector response function versus energy, incident beam intensity

Secondary Fluorescence Enhancement

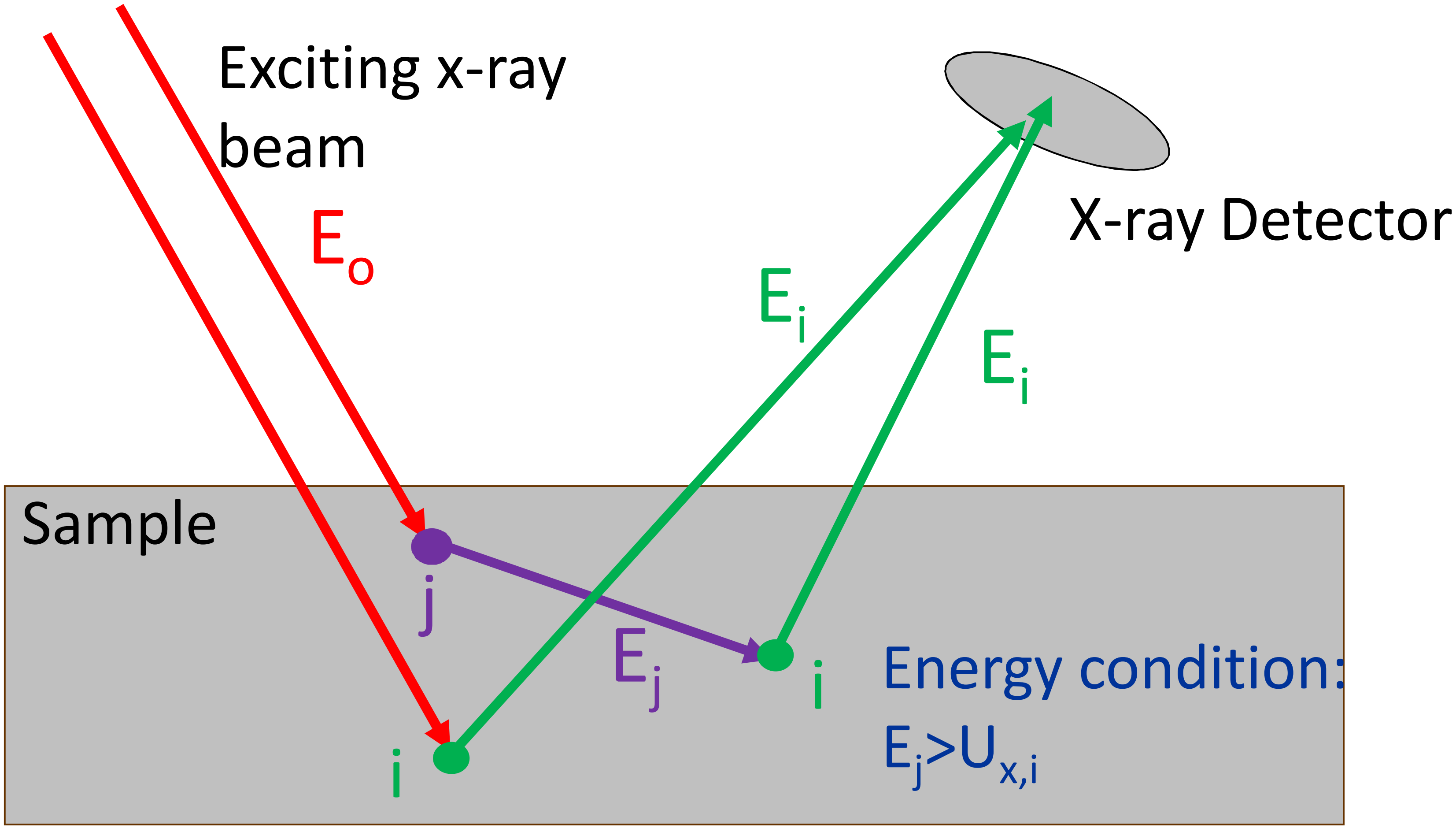

Element ***j*** characteristic x-ray(s) can excite element ***i*** characteristic x-rays within the sample volume

Photo-/Auger/Compton e⁻ Indirect XRF intensity

Electron spectrum:

Discrete: Photo-e, Auger

Continuous: Compton

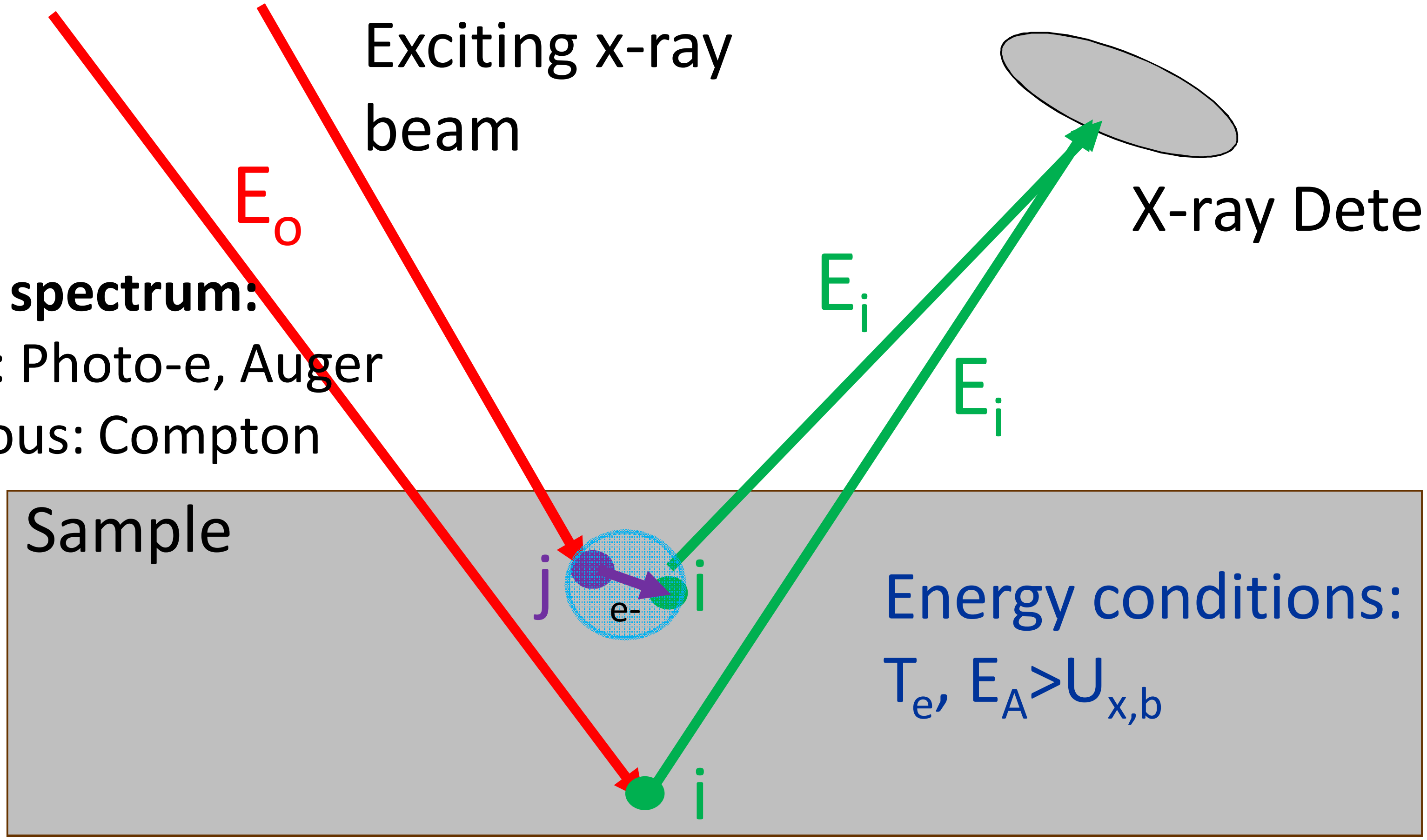

Ejected electrons from the atoms of element ***j*** can ionize an inner shell of element ***i***

N. Kawahara in Handbook of Practical X-Ray Fluorescence Analysis, J. Fernandez et *al.*, X-Ray Spectrometry 2013, 42, 189–196, K. Stoev, J. Phys. D: Appl. Phys. 25 (1992) 131-138

Chain of XRF related Fundamental interactions

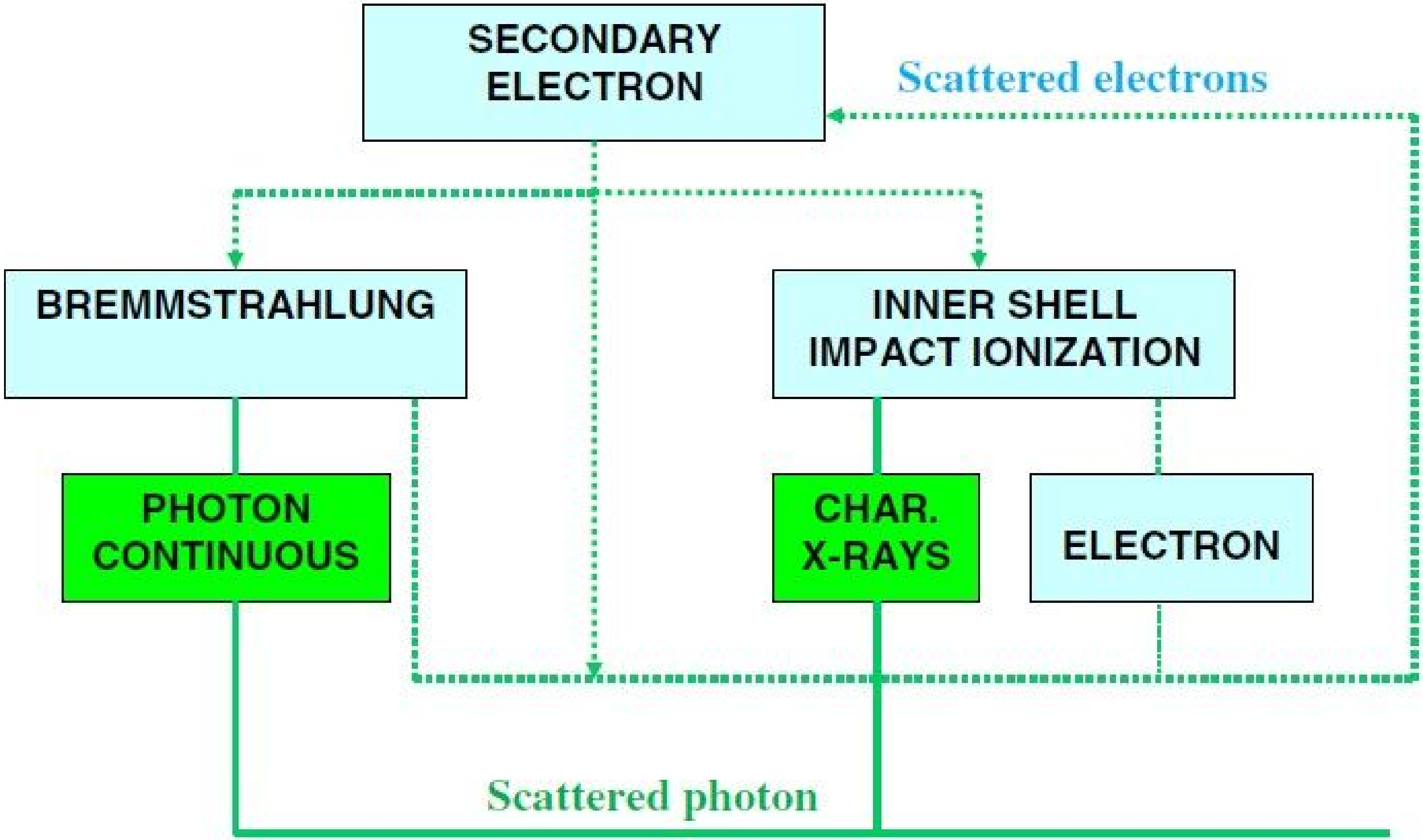

J. Fernandez et *al*., X-Ray Spectrom. 2013, 42, 189–196

XRF intensities for non-parallel x-ray beams

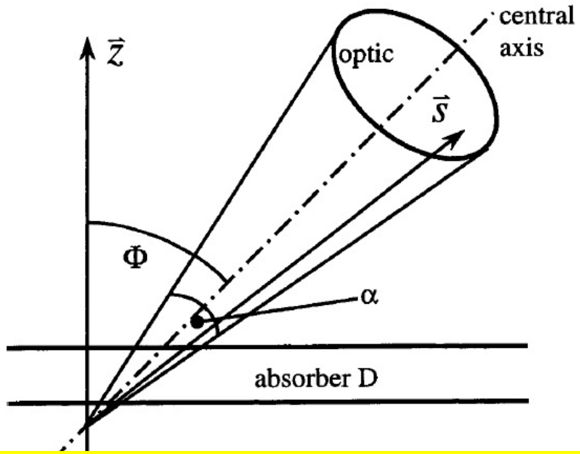

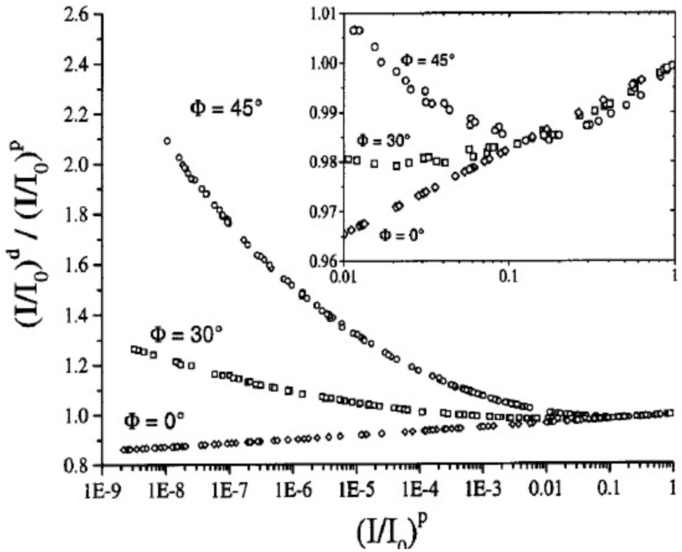

The divergent angle is 20° and the trajectories are distributed isotropically

$$\left(\frac{I}{I_0}\right)^d = \int p(\vec{s})exp\left(\frac{-\mu\rho D}{s_z}\right)d\vec{s}$$

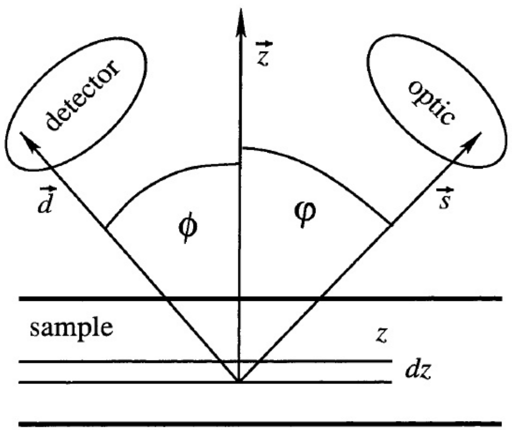

Beam divergences is taken into account by 'equivalent angles' calculated with Monte Carlo integration

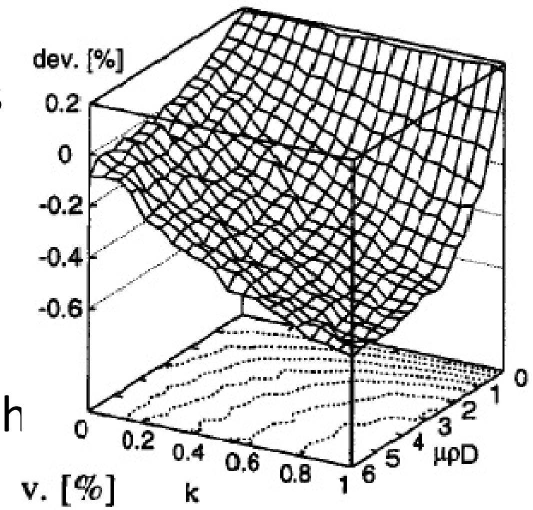

Polycapillary lens: divergent angle of 10°, perpendicular to the sample surface. Detector angle: 20°.

W. Malzer, B. Kanngiesser, X-Ray Spectrom. 2003; 32: 106–112

Surface Topography in XRF intensities

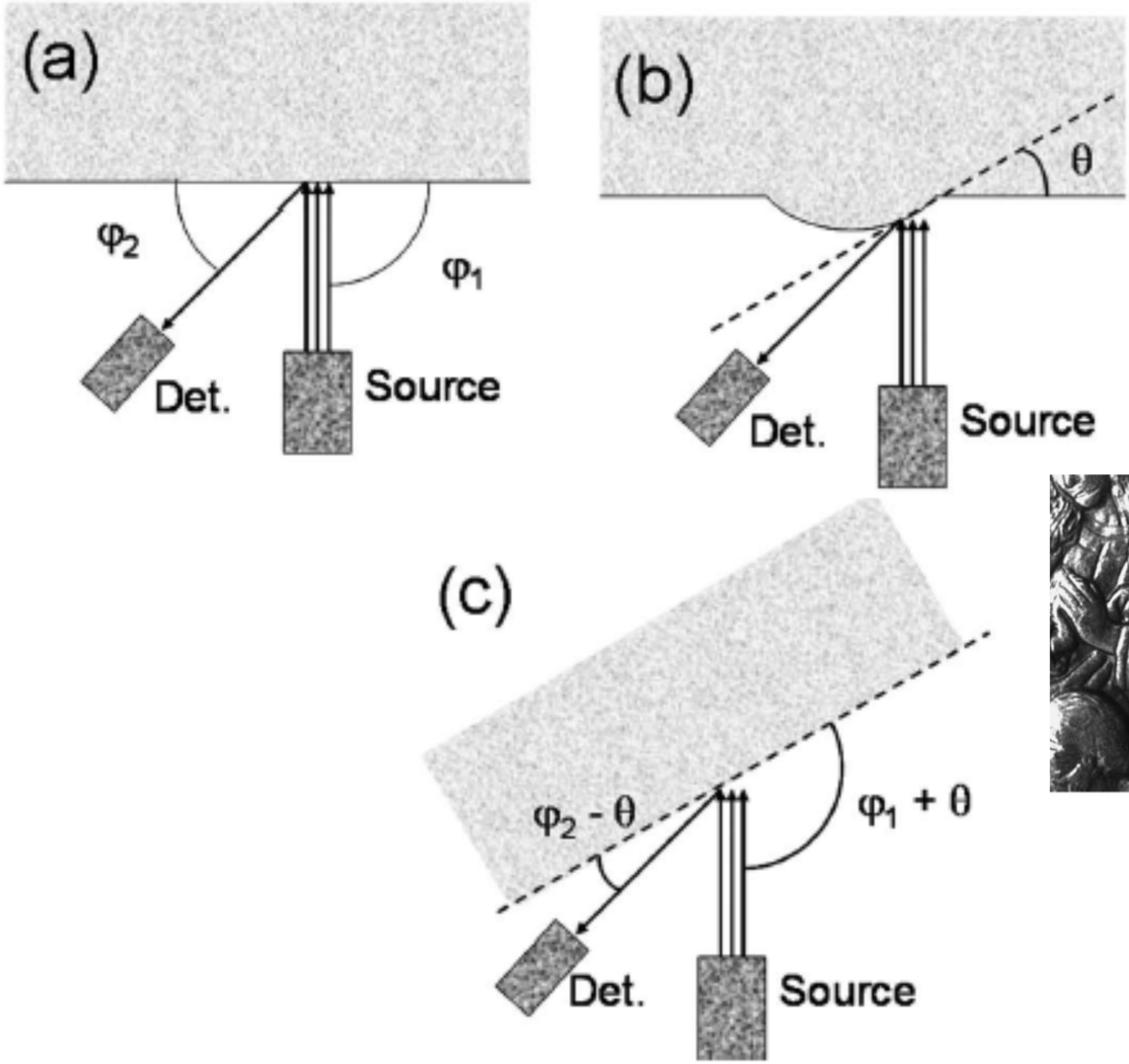

T. Trojek, J. Anal. At. Spectrom., 2011, 26, 1253

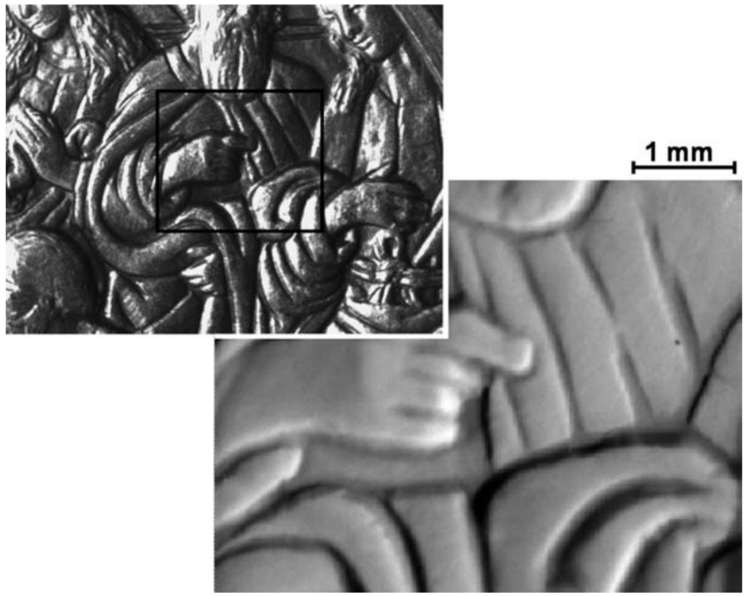

Surface Topography in XRF intensities

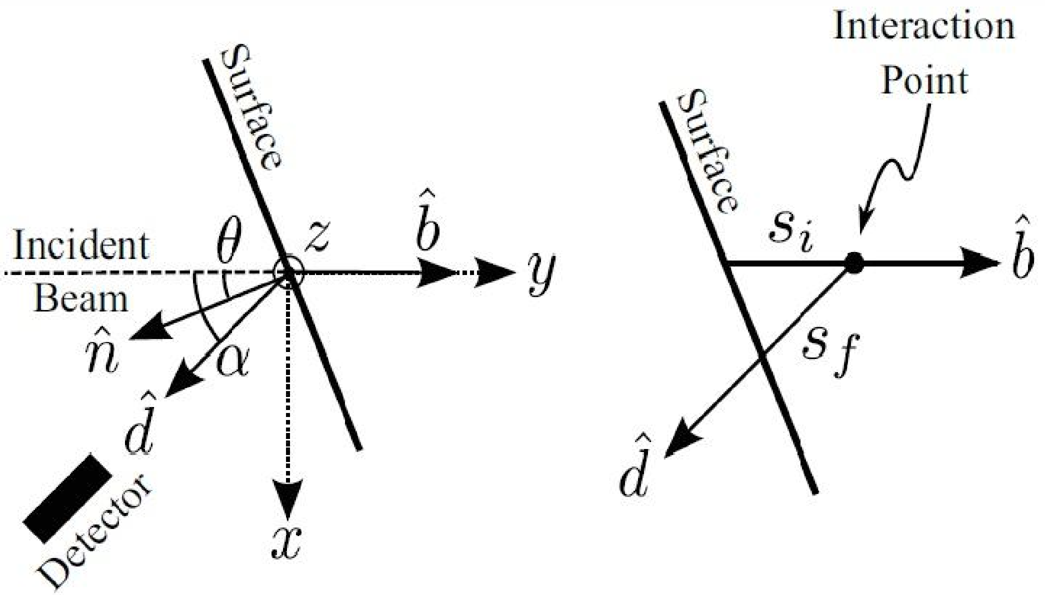

$$I(\theta) \propto \frac{1}{1 + \left(\mu_f / \mu_i\right) (\cos a + \tan\theta \sin a)^{-1}}$$

E. C. Geil and R. E. Thorne, J. Synchrotron Rad. (2014), 21, 1358

ϑ, *α* are the rotation angles of the surface=be normal and detector axis, respectively, around the perpendicular *z* axis defined with respect to y-axis; *ϑ* = 0 for a surface parallel to the *xz* plane

Surface Topography in XRF intensities

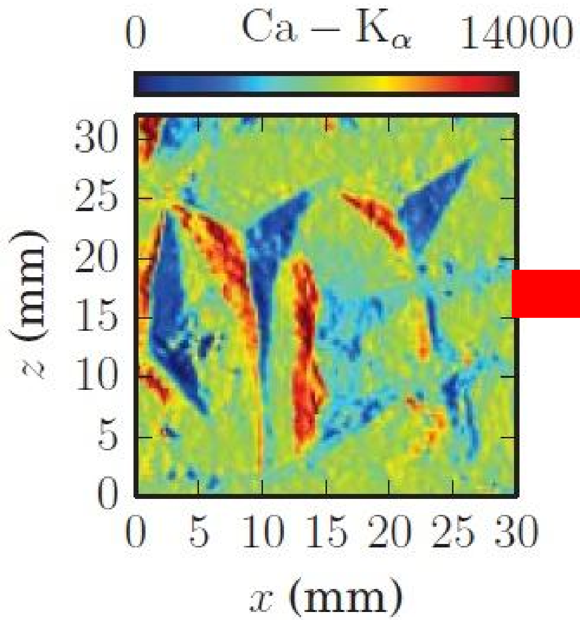

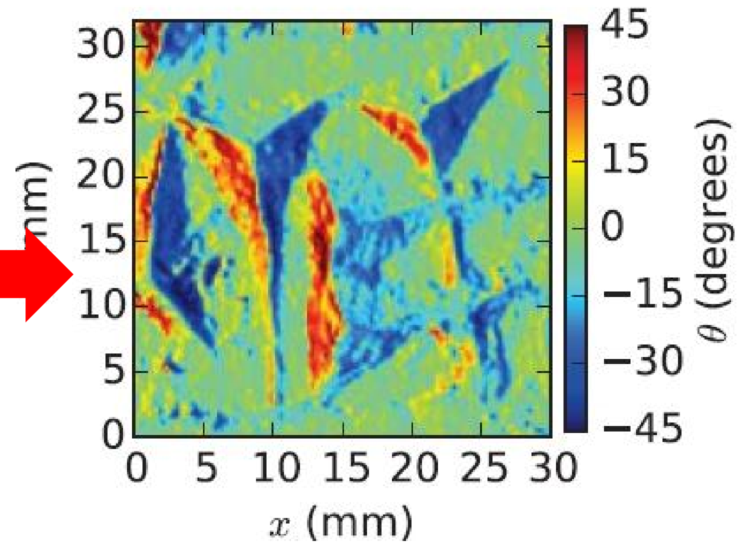

Map of surface angle θ computed from the Ca – Kα fluorescence

Rendering of the scanned area and shaded as if obliquely illuminated from the right side by a light source.

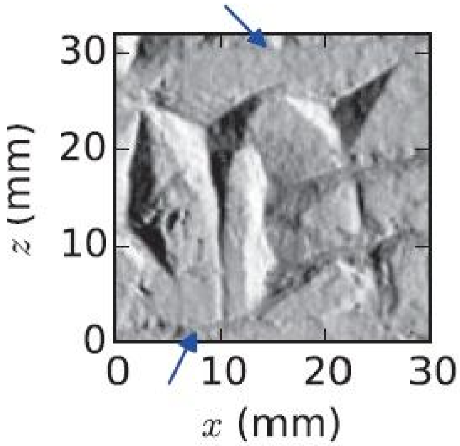

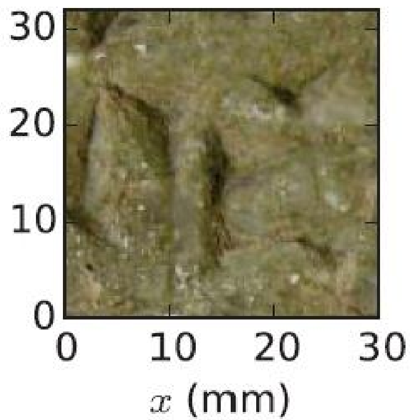

Photograph of the scanned area, adjusted to enhance contrast and brightness.

Surface Topography in XRF imaging

Hint -1 :

For samples with appreciable surface relief, an optimum approach is to orient the sample's 'mean" normal along the beam direction (theta =0)

Hint 2: The angle effect vanishes as the detector position approaches the incident beam (smaller α), and it is maximal when the detector is perpendicular to the beam

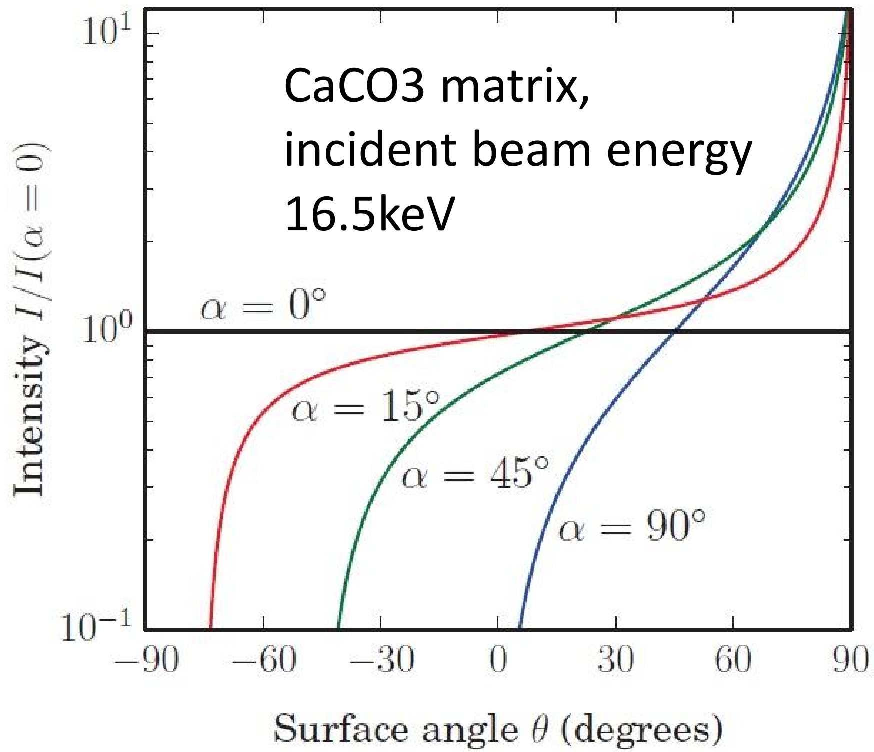

Hint -3

The stage should be aligned across the perpendicular to the incident beam plane, otherwise it will produce distortion of the images (the interaction point will vary not symmetrically)

MAXRF- FFXRF spectrometers

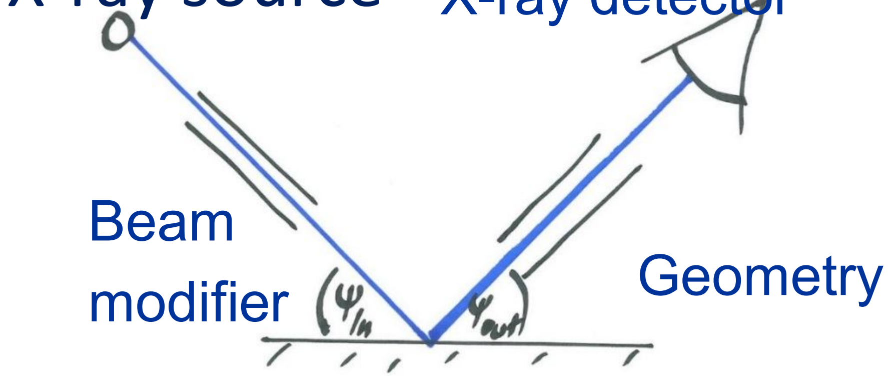

F.F. P. Romano et al., Analytical Chemistry 2014, 86, 10892

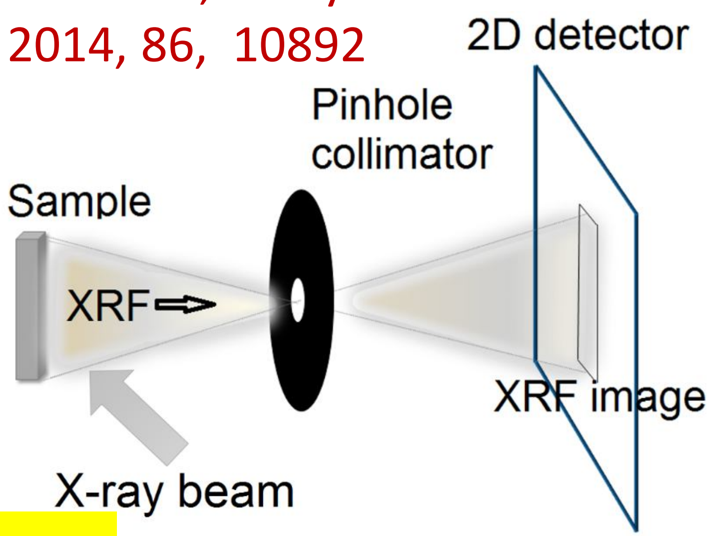

F.P. Romano et. al. JAAS 2017
DOI: 10.1039/c6ja00439c

FF-XRF

- Radiation dose
- Motor control

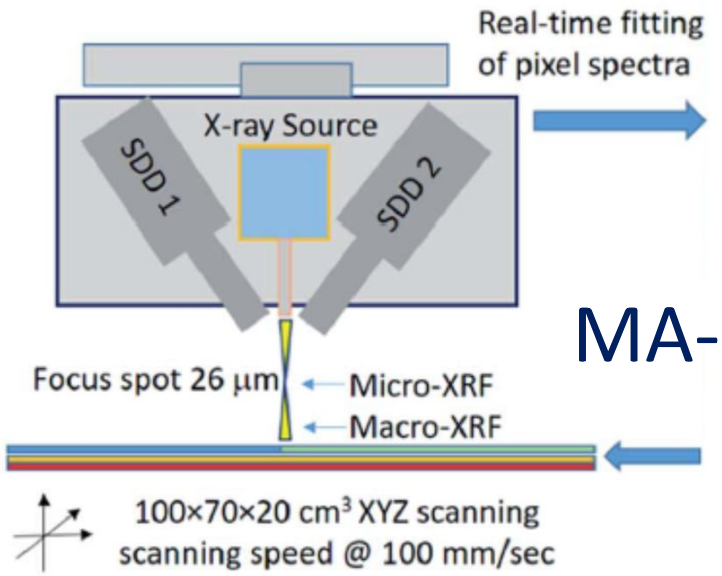

MA-XRF

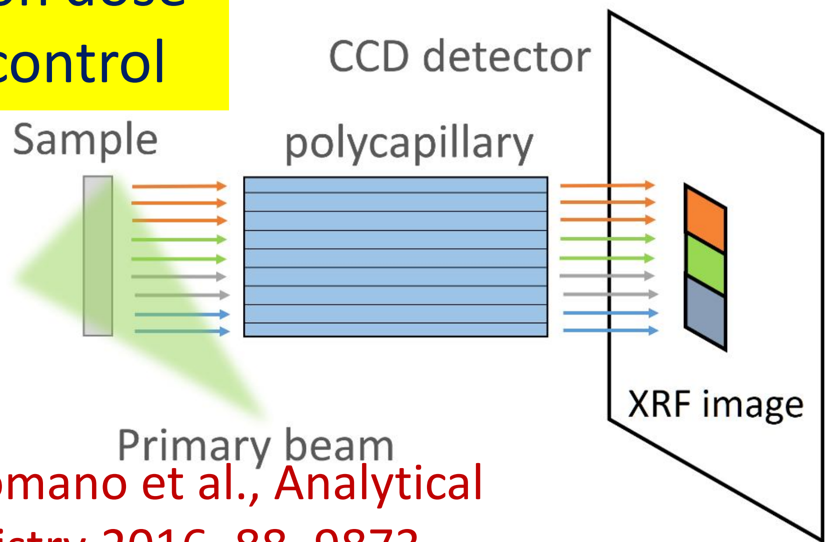

F.P. Romano et al., Analytical Chemistry 2016, 88, 9873

X-ray sources

Synchrotron radiation

High brilliance, polarization:
Micro/Nano-XRF (< 1µm)

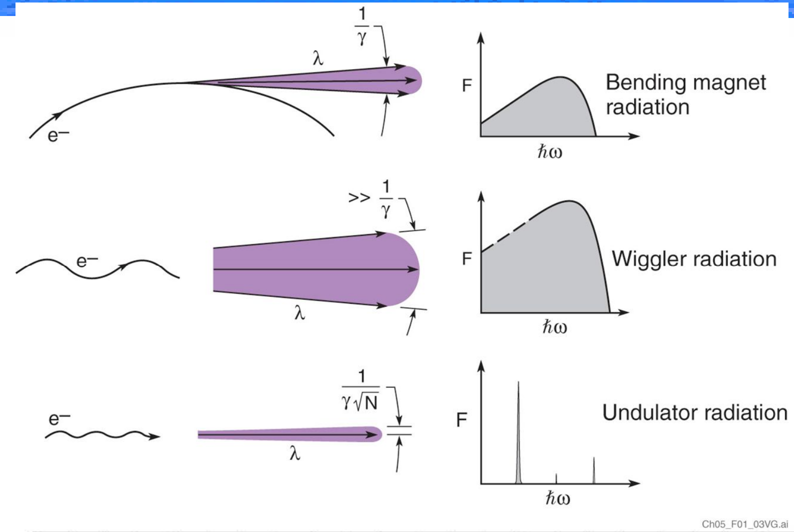

X-ray tubes

- High power (~ kW) diffraction x-ray tubes
- Micro focus (~ 50-100µm) anode size - Brilliance optimised (30-50 W (air cooled)
- Miniature X-ray tubes – geometry optimized (2W-12W, 50kV)

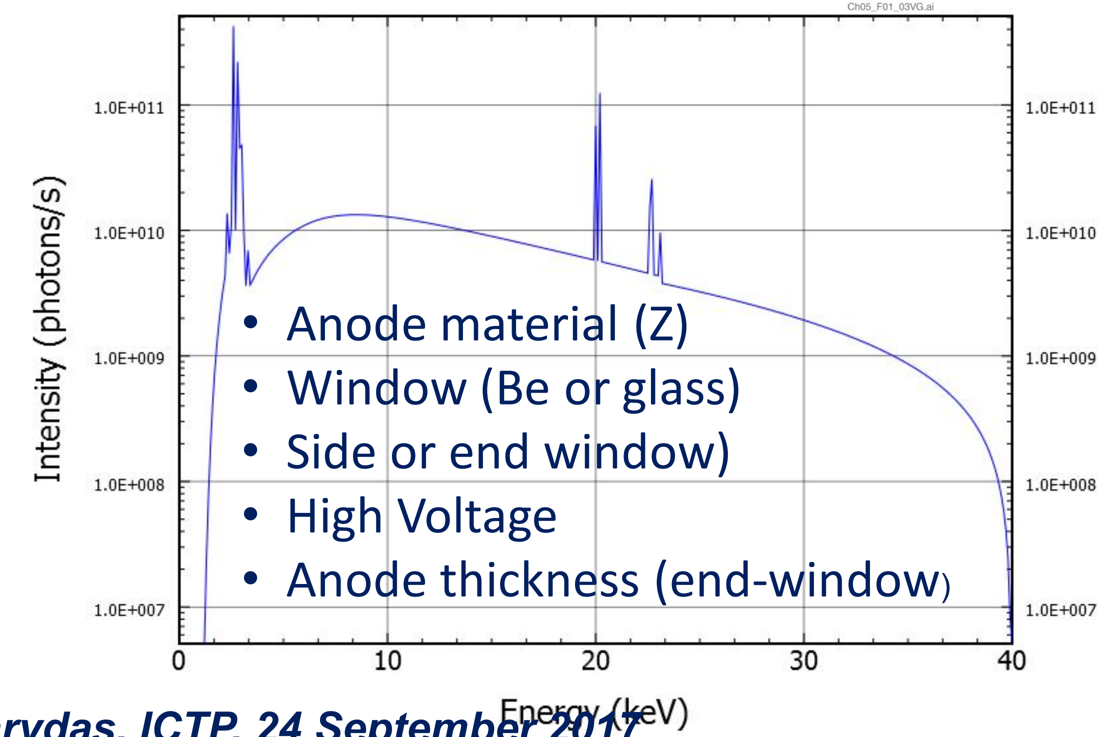

- Anode material (Z)
- Window (Be or glass)
- Side or end window)
- High Voltage
- Anode thickness (end-window)

Low/High power X-Ray Sources

Oxford Model: XTF5011

Anode materials: Rh, Ag, Mo
Focus spot size 50-150 µm
Exposure < 0.5 mR/hr

Moxtek end/side window tubes, 10W, 50kV

Newton M47, 50kV 10W X-ray Source, 400 grs

Quantification in Tube excited XRF analysis

Fe excitation

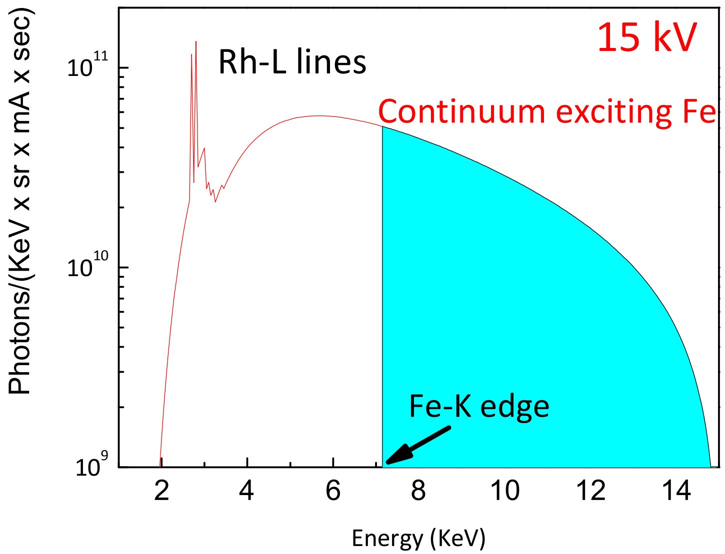

Si excitation

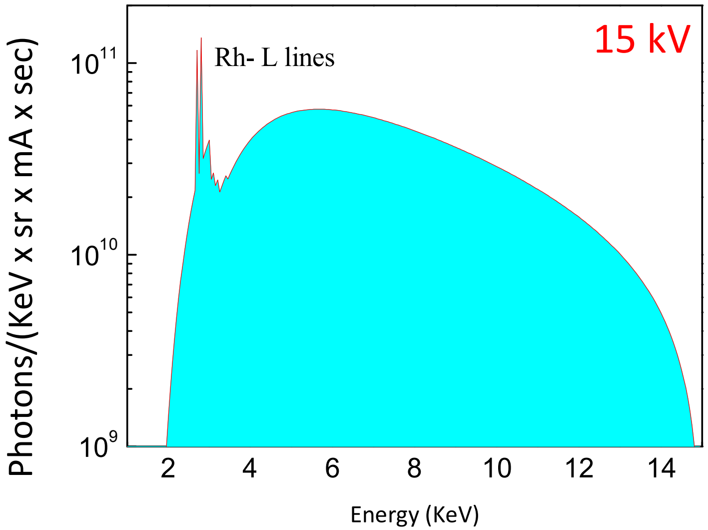

15 kV
Unfiltered

Cu excitation

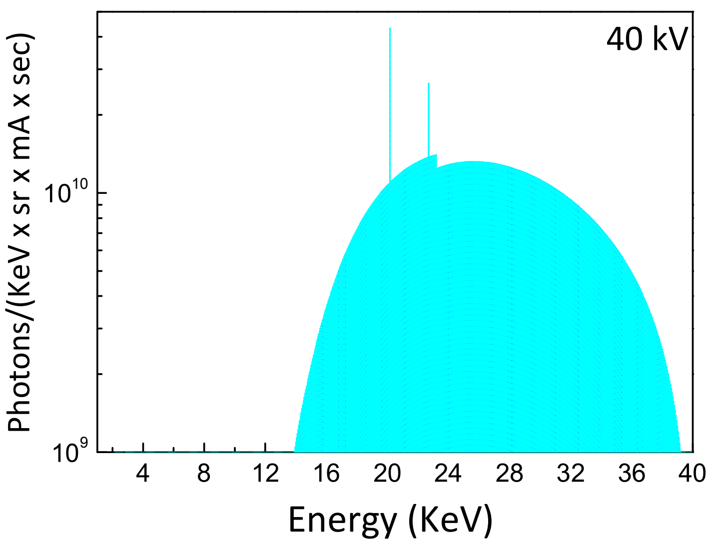

Ag excitation

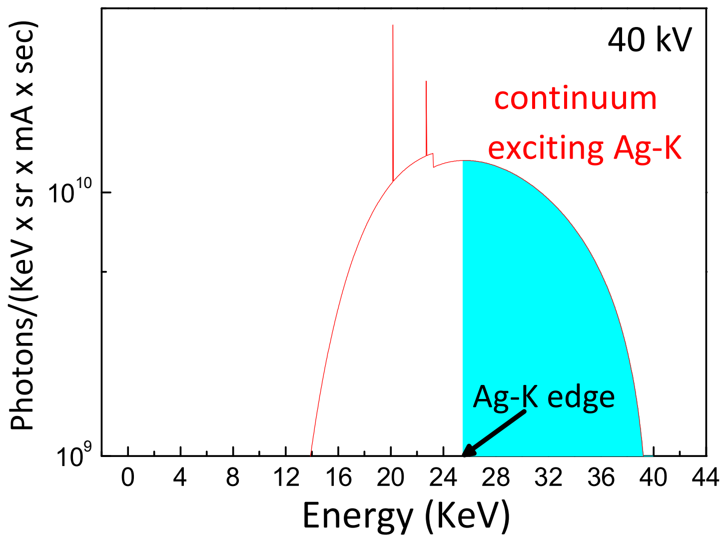

40 kV
Filtered

Beam Modifier

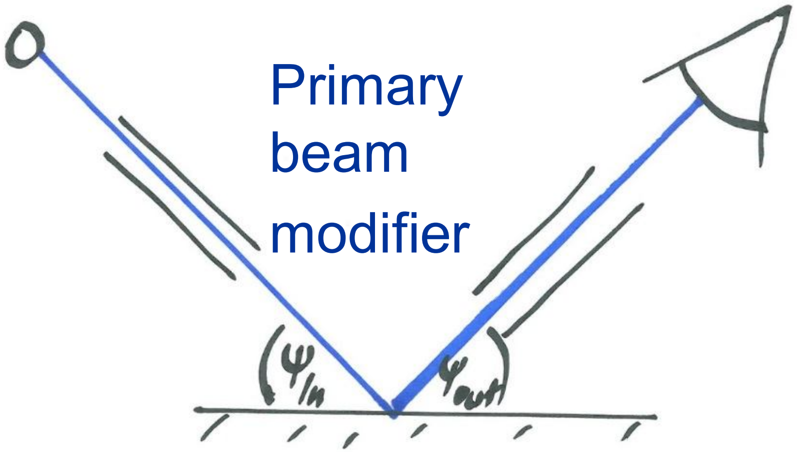

The modifier device (for either beam divergence, focusing, spectral distribution) can be:

- ❑ **Collimator**
- ❑ **Filter**
- ❑ **Monochomator**
  - Secondary target
  - Multilayer/crystals
- ❑ **Optics**
  - Focusing crystals
  - Capillary lenses

To improve:

- ➢ Monochomaticity or P/B ratio
- ➢ Beam spot size spatial resolution
- ➢ Polarization state of incoming radiation
- ➢ To eliminate the presence of **diffraction peaks**

Filtered vs Unfiltered excitation: An example

Rh anode tube, 40 kV, low atomic number scatterer

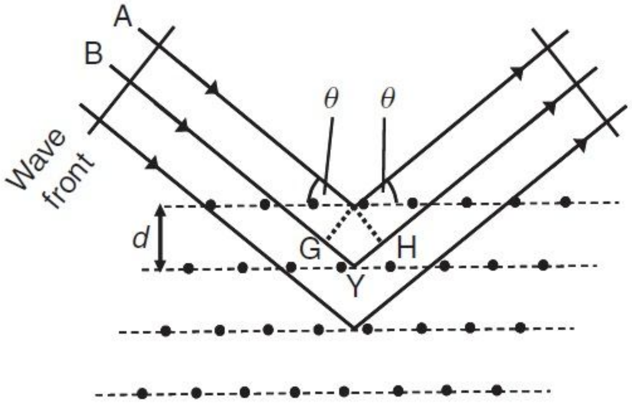

$$n\lambda = 2 \cdot d \cdot \sin\theta$$

$$E = \frac{hc}{\lambda}, E(keV) = \frac{1.2398}{\lambda(nm)}$$

Bragg's Law

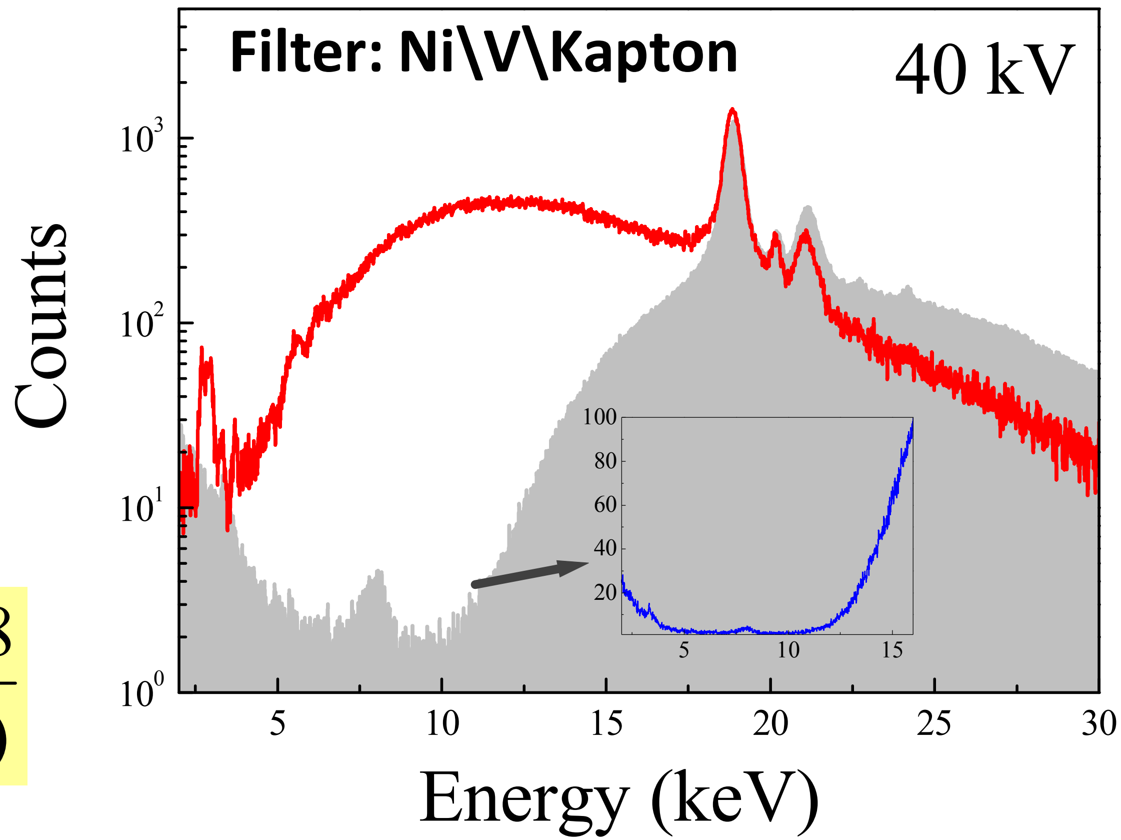

@ 19 keV: 3-4 times

@ 5-15 keV: 10-100 times

Filtered vs Unfiltered excitation: An example

LANDIS MA-XRF spectrometer

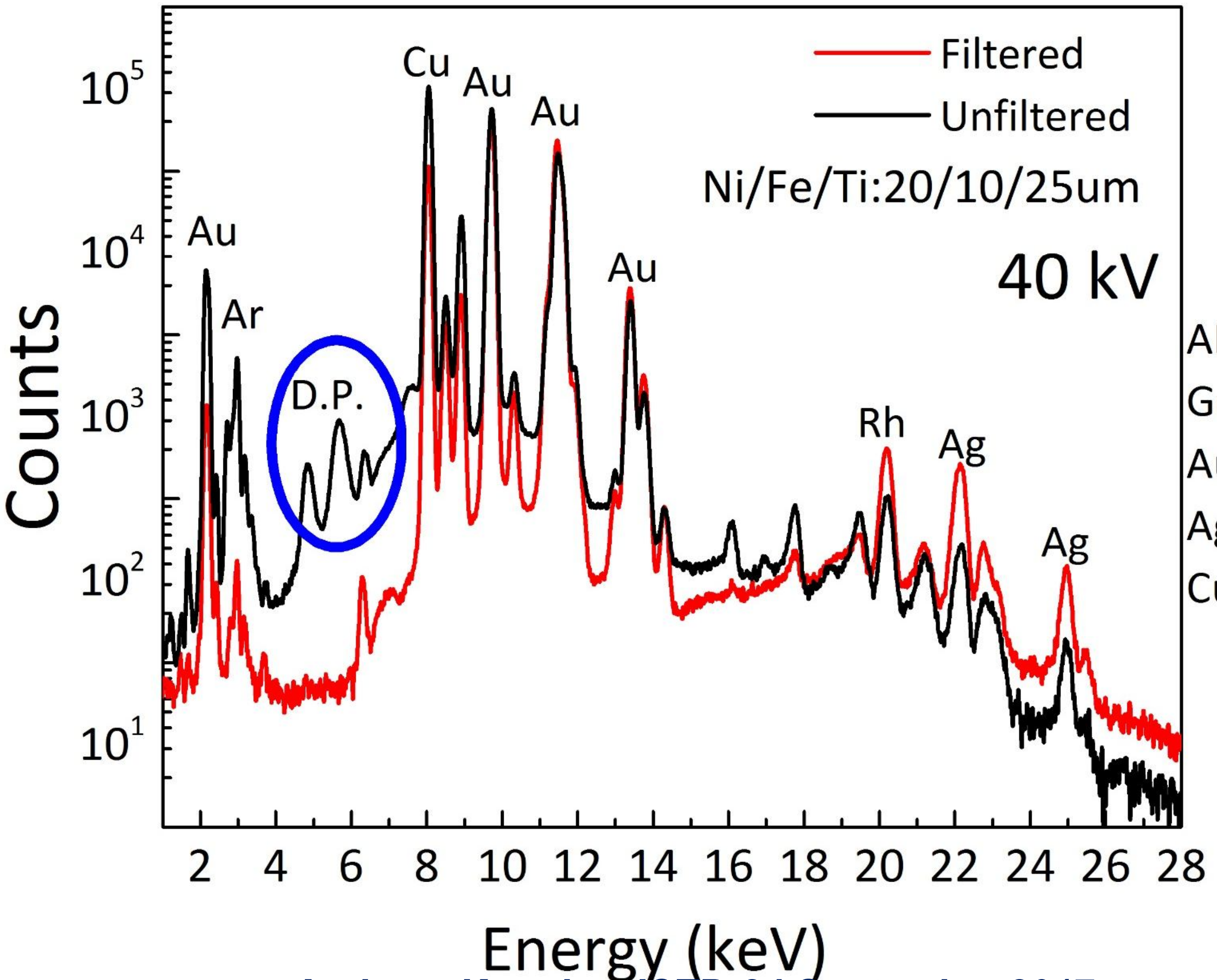

AB-LLI
Gold Alloy
Au: 74.96%
Ag: 5.04%
Cu: 20.2%

X-ray Optics in MA-XRF analysis

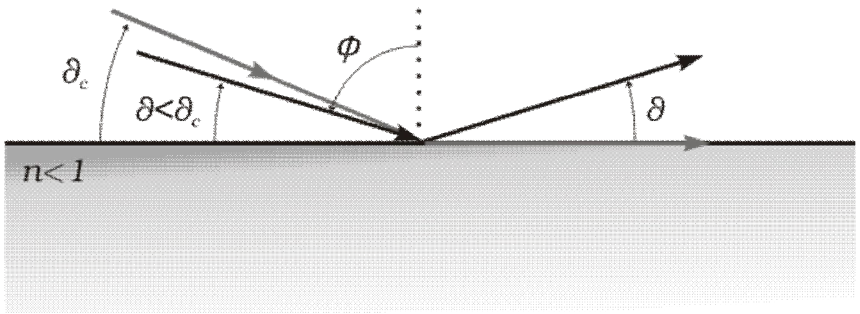

$$n \approx 1 - \delta$$

$$\vartheta_{crit} = \sqrt{2\delta}$$

$$\vartheta_{crit}(degrees) \approx \frac{1.651}{E(keV)} \sqrt{\frac{Z}{A}\rho\left(\frac{g}{cm^3}\right)}$$

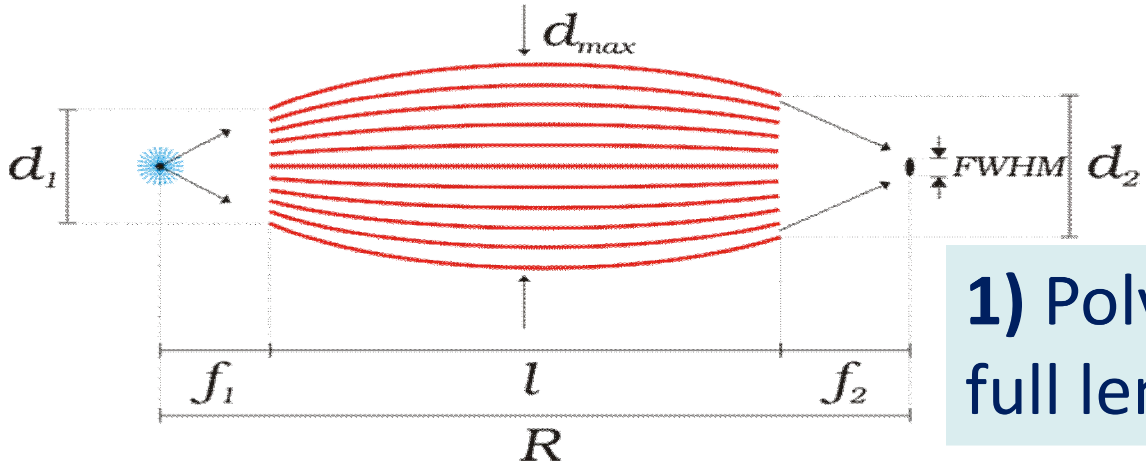

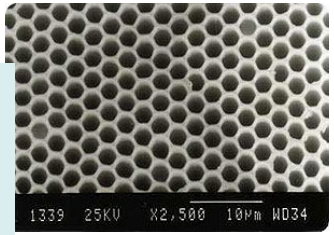

1) Polycapillary full lens

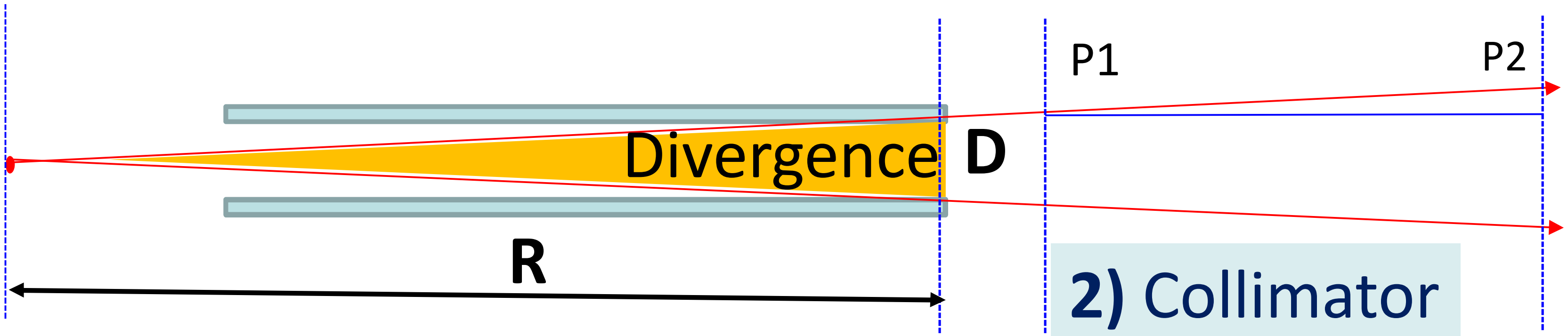

2) Collimator

Characteristics of Polycappilary X-ray lenses

- Spot size –FWHM (E)
- Gain Factor – G(E)
- Focal distance

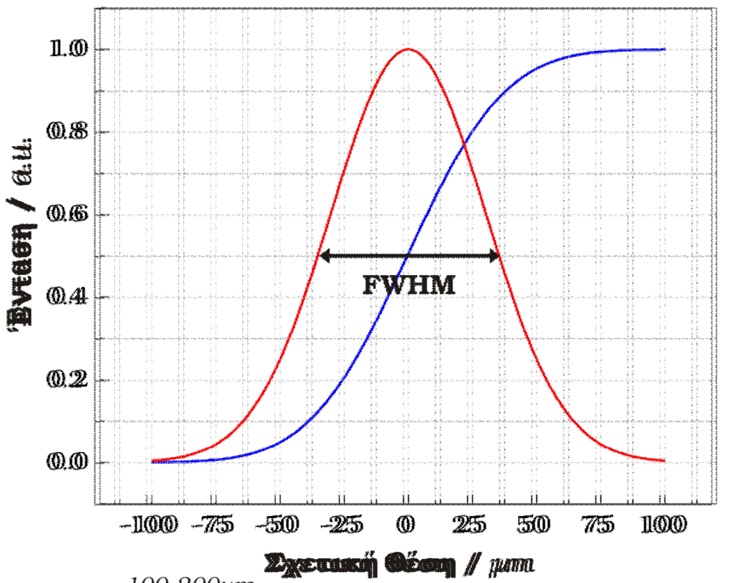

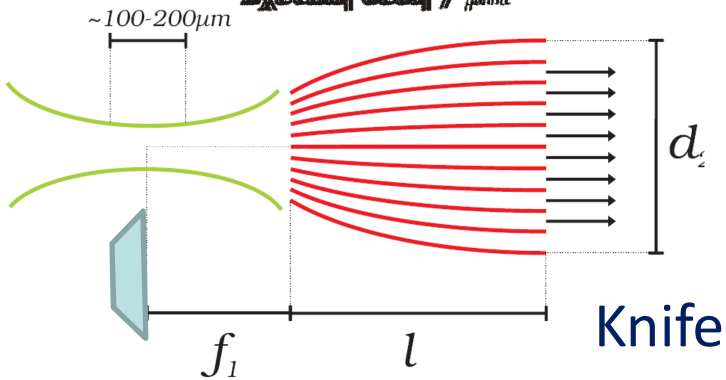

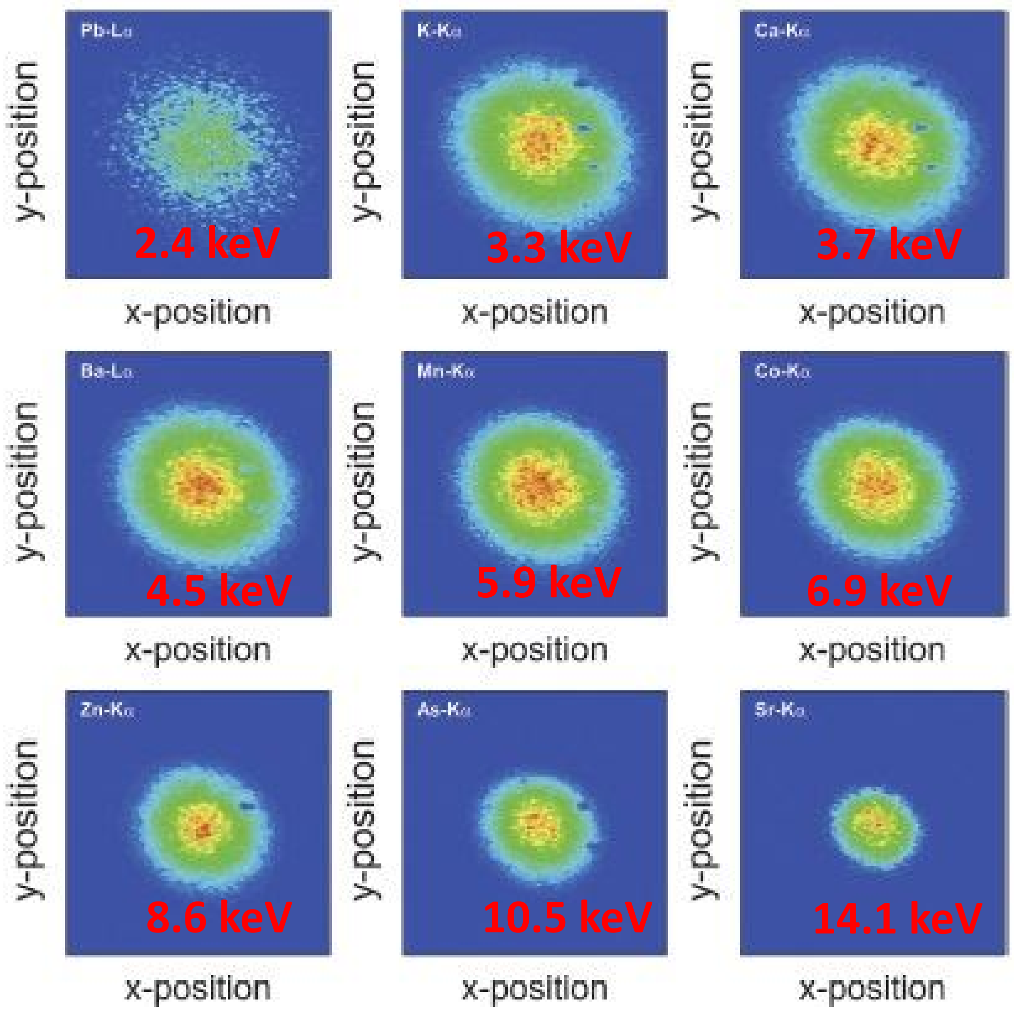

T. Wolff et al, JAAS, 2009 24 669

Knife edge scan

Characteristics of Polycappilary X-ray lenses

- Spot size –FWHM (E)
- Gain Factor – G(E)
- Focal distance

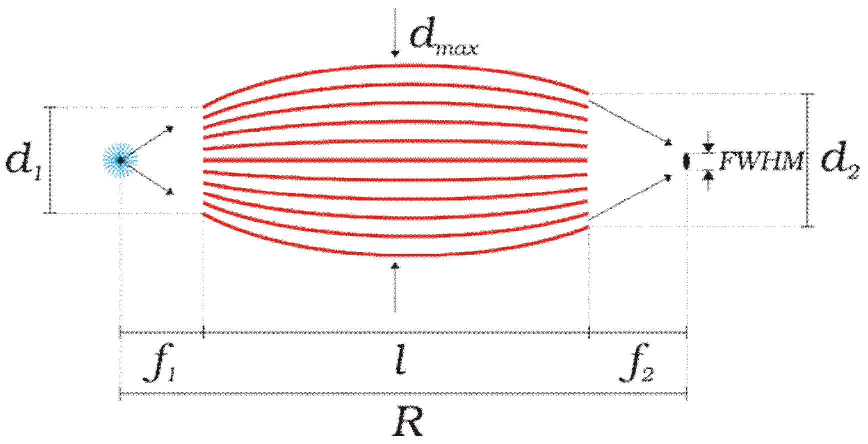

$$G(E) = \frac{\Phi_{lens}}{\Phi_{col}} = \frac{T(E) \cdot d_{in}^2 \cdot R^2}{[FWHM(E)]^2 \cdot f_1^2}$$

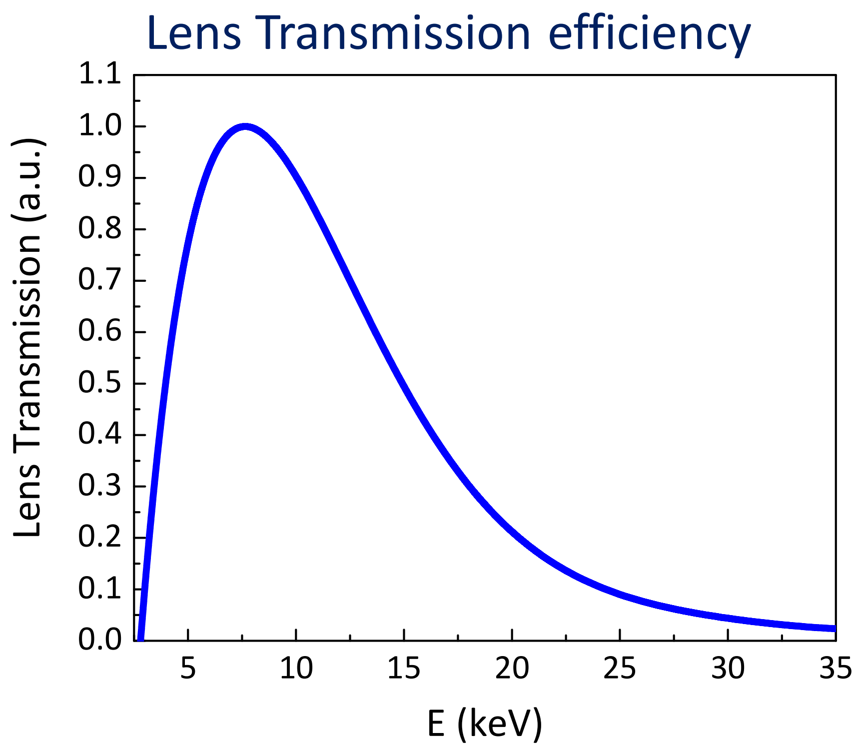

V. Kantarelou, A.G. Karydas,
XRS 2016, DOI 10.1002/xrs.2661

Characteristics of Polycappilary X-ray lenses

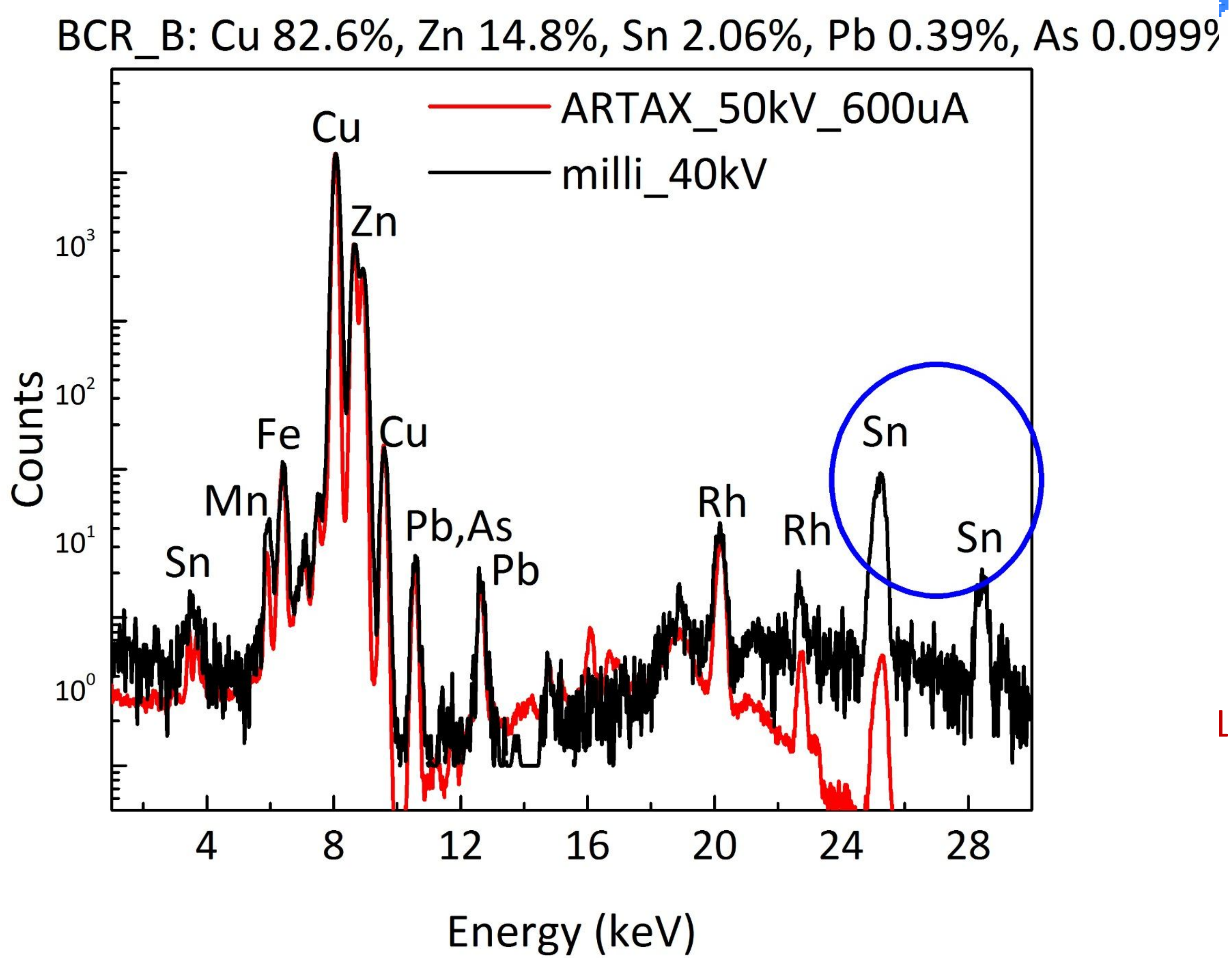

d

L

Characteristics of Polycappilary X-ray lenses

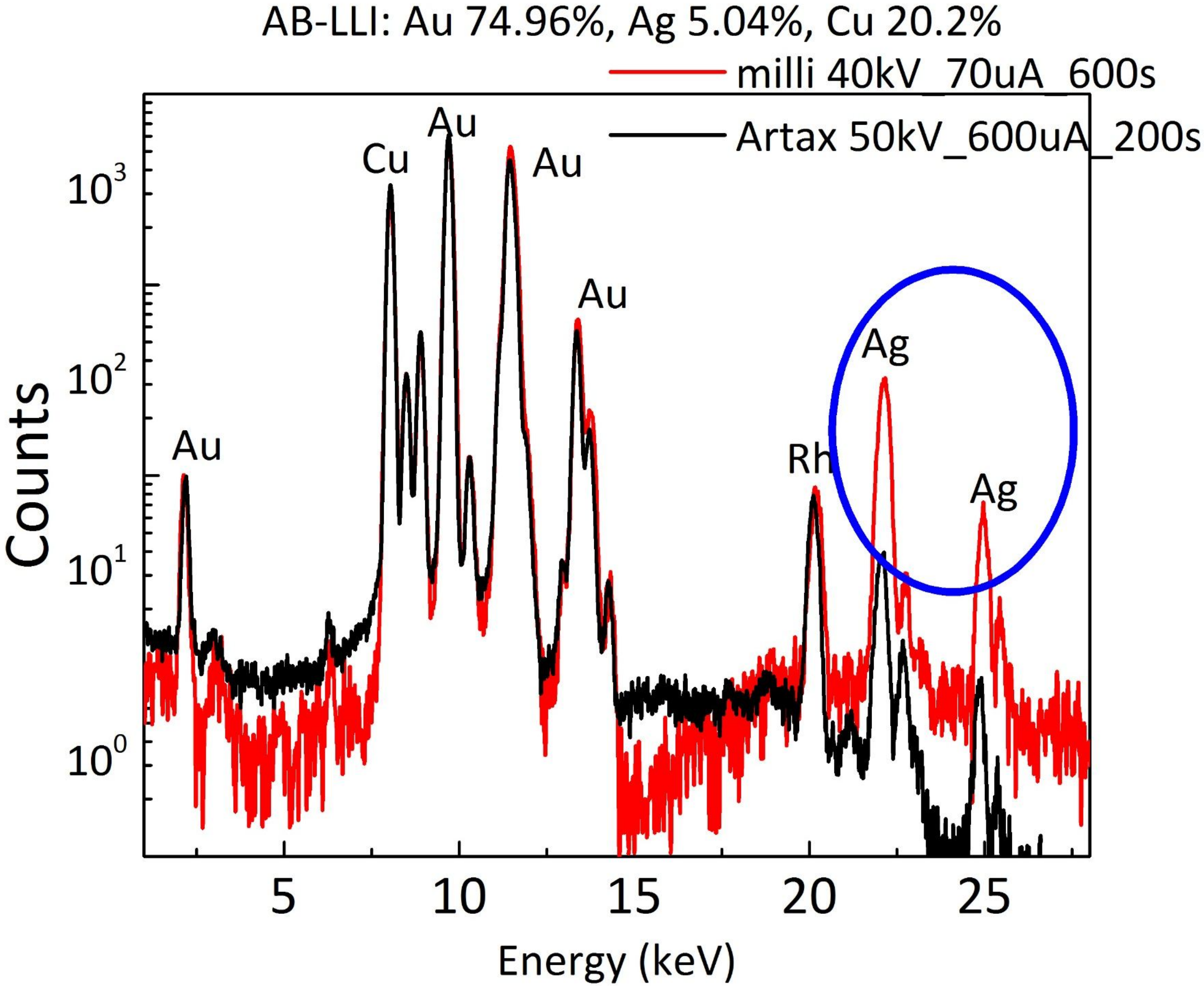

Characteristics of Polycappilary X-ray lenses

- Spot size –FWHM (E)
- Gain Factor – G(E)
- Focal distance

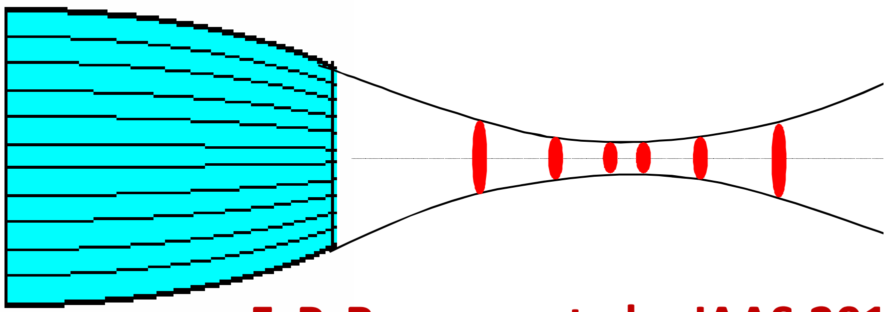

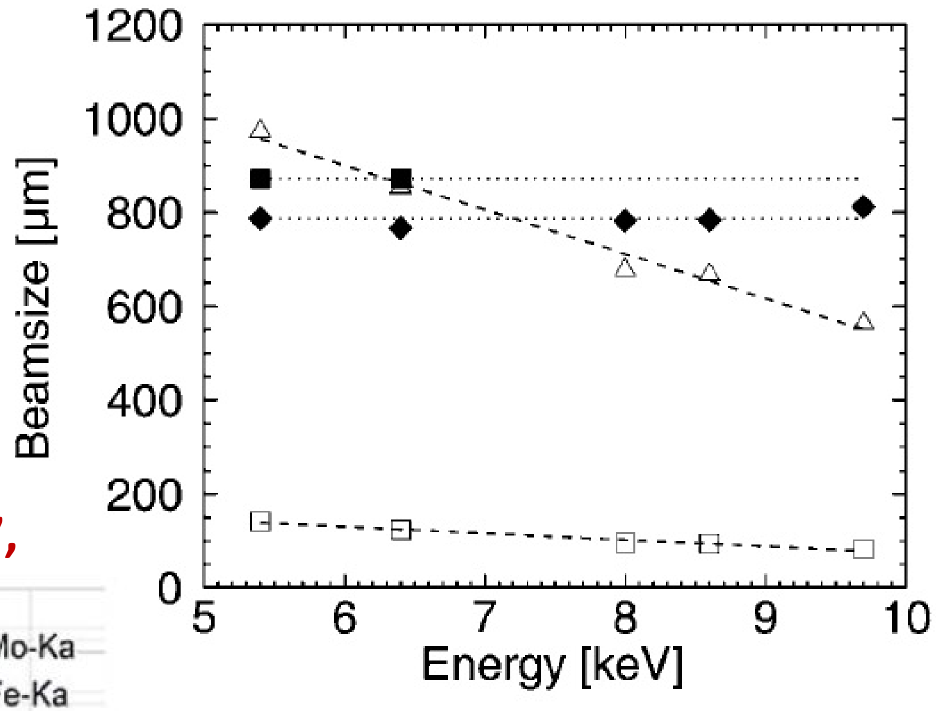

F. P. Romano et al., JAAS 2017, DOI: 10.1039/c6ja00439c

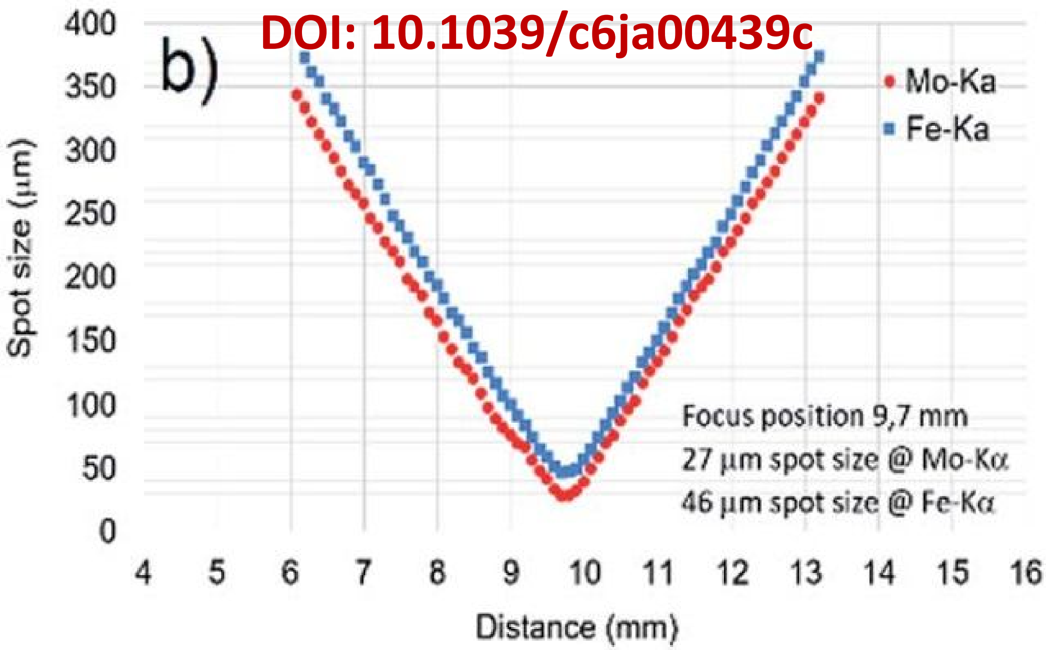

M. Alfeld et al., JAAS 2011, 26, 899

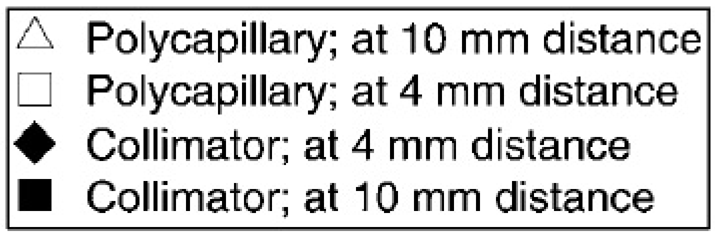

Physics & technology behind X-rays detection

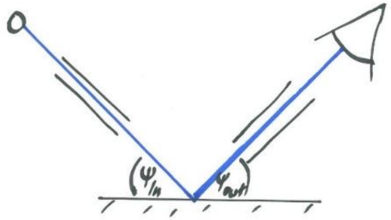

- ❑ A photon produces pairs of free electrons and holes (energy needed to create an electron-hole pair=3.6 eV)
- ❑ Charge is collected from the depleted active region of the sensor and it is further amplified
- ❑ Signal strength is proportional to the detected photon energy

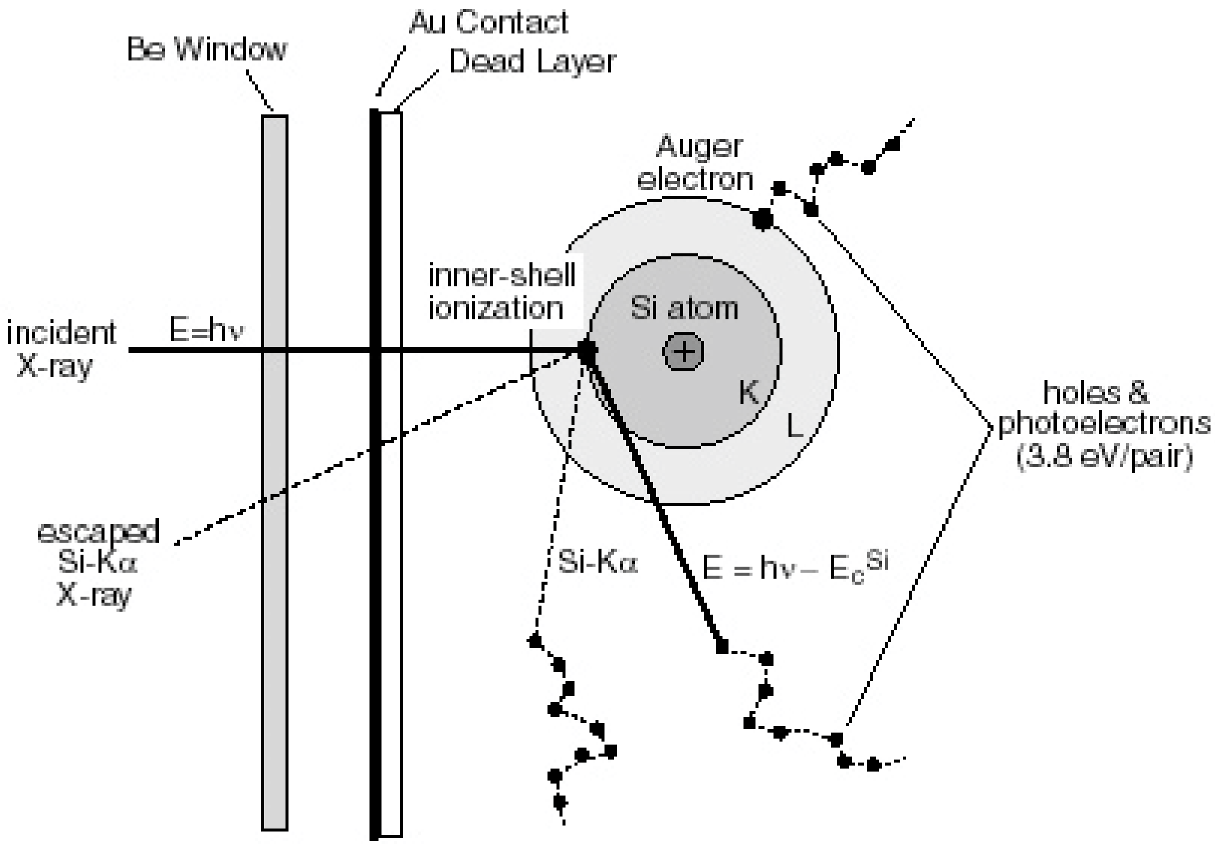

Physics & technology behind X-rays detection

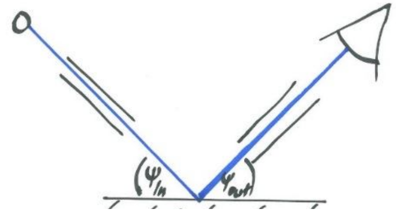

- A photon produces pairs of free electrons and holes (energy needed to create an electron-hole pair=3.6 eV)
- Charge is collected from the depleted active region of the sensor and it is further amplified
- Signal strength is proportional to the detected photon energy

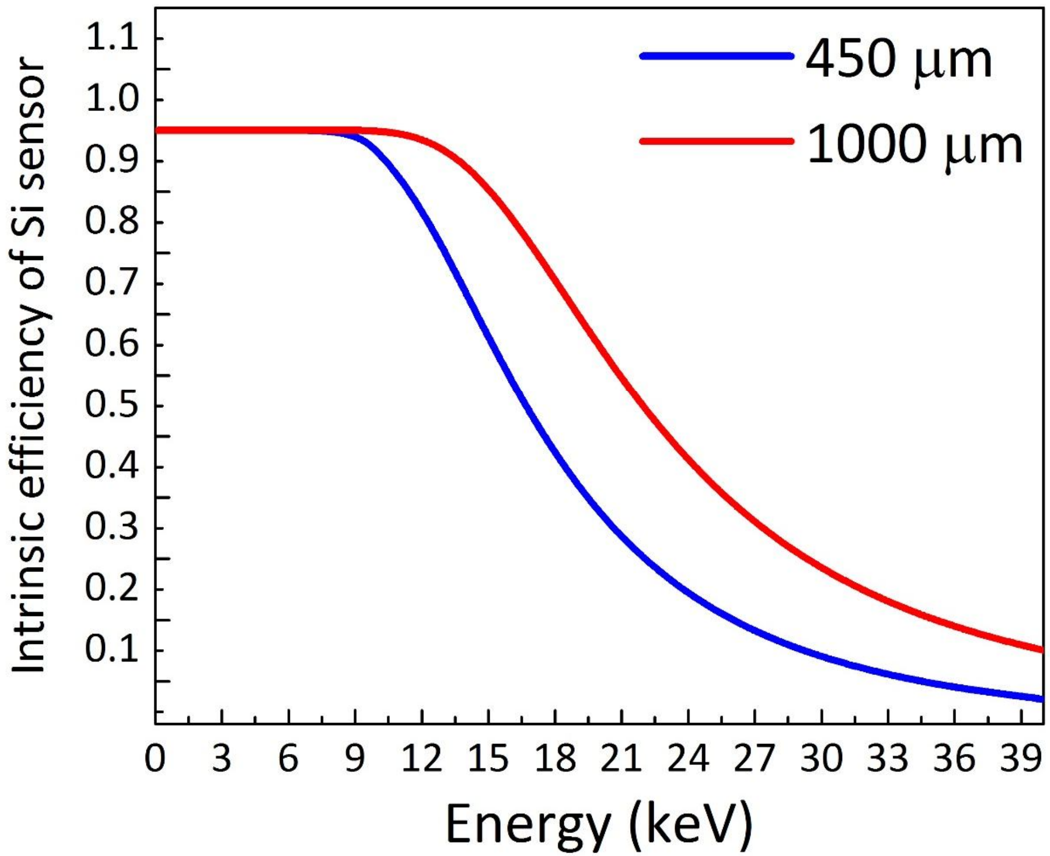

Physics & technology behind MAXRF imaging

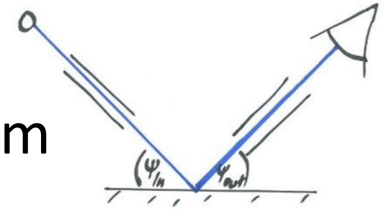

Silicon Drift Detector - Principle: The charge is drifted from a large area into a small read-out node with low capacitance, independent of the active area of the sensor. Thus, the serial noise decreases and shorter shaping time can be used

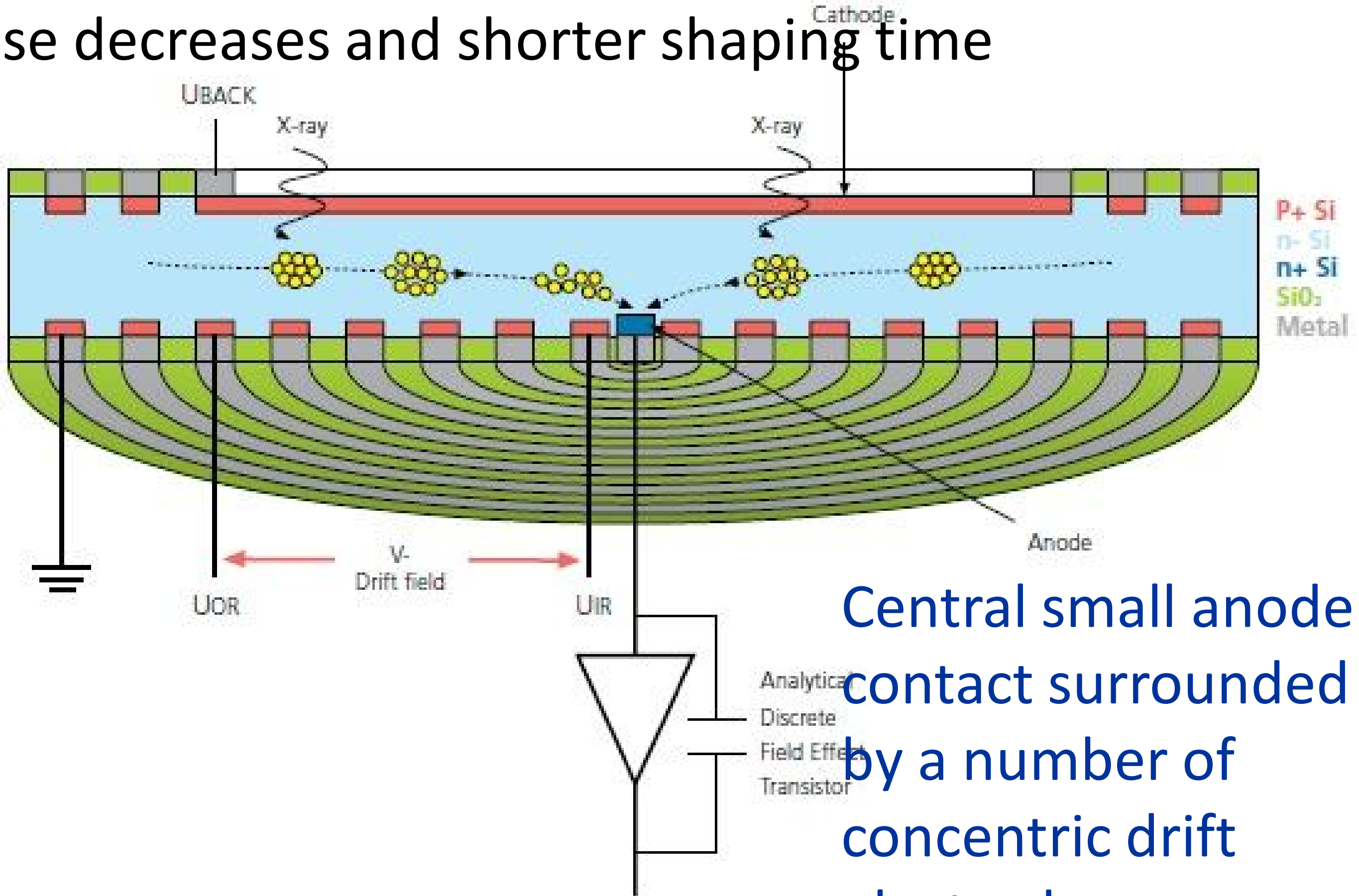

Two advantages:

1) Faster counting is enabled
2) Higher leakage current can be accepted, drastically reducing the need for cooling

Central small anode contact surrounded by a number of concentric drift electrodes

Figure from Oxford Instruments Manual

Performance Figures of Silicon Drift Detectors

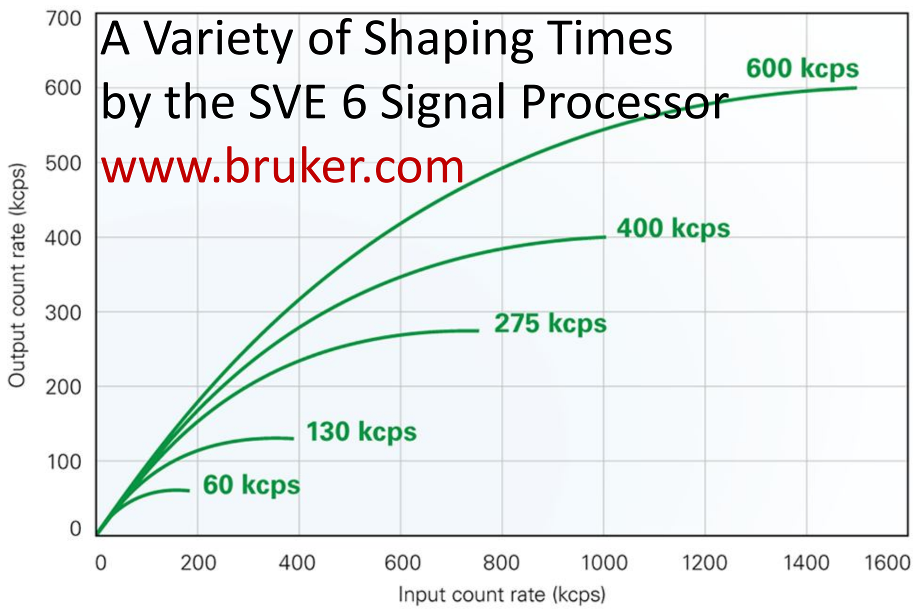

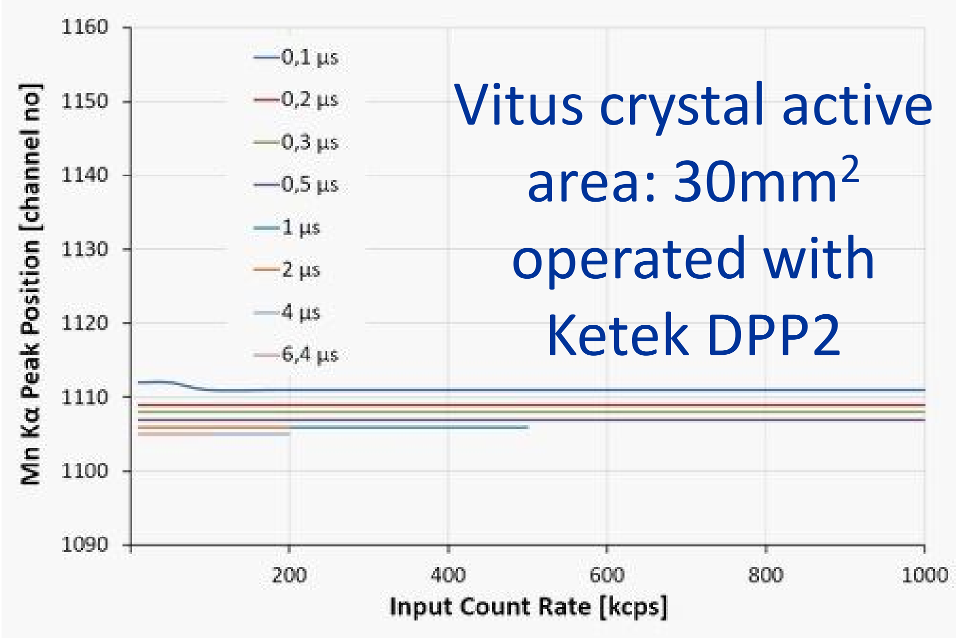

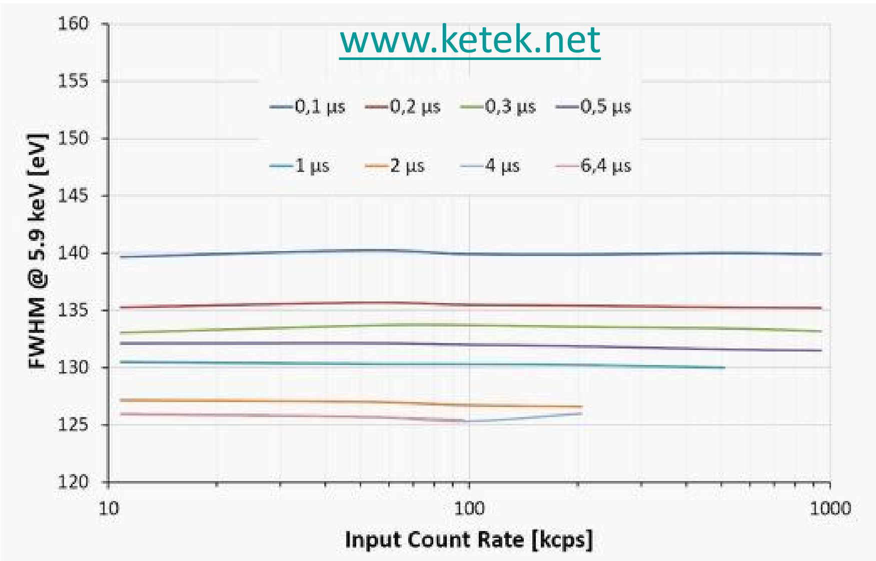

CUBE preamplifier supports high-rate spectroscopy in XRF mapping applications while preserving enough energy resolution at shorter shaping times.

Bombelli et al, DOI: 10.1109/NSSMIC.2012.6551138, 2012

The use of short peaking times further reduces the impact of the detector leakage current on the total noise. Room temperature operation!

Performance Figures of Silicon Drift Detectors

Vitus crystal active area: 30mm^2 operated with Ketek DPP2

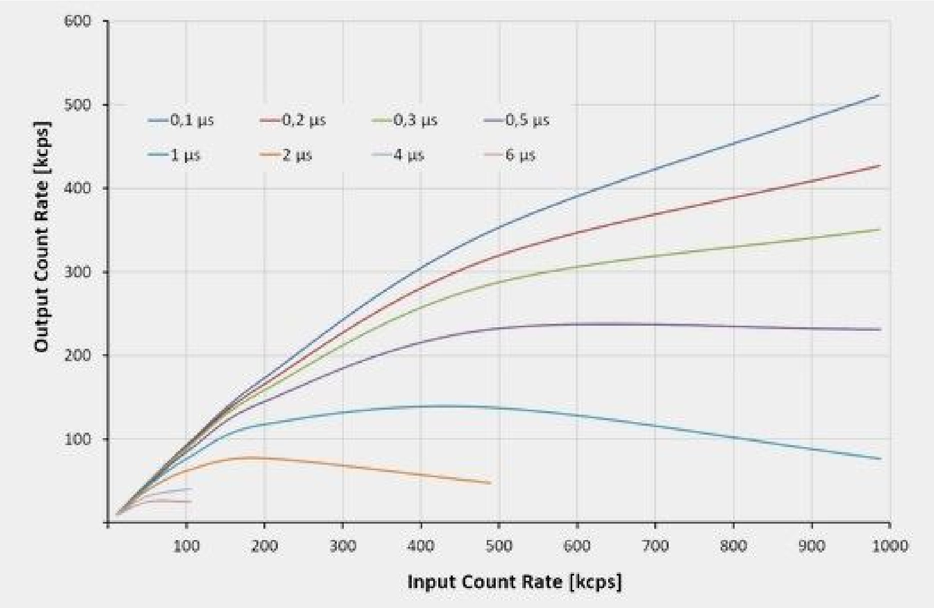

Vitus crystal active area: 80mm^2 operated with Ketek DPP2

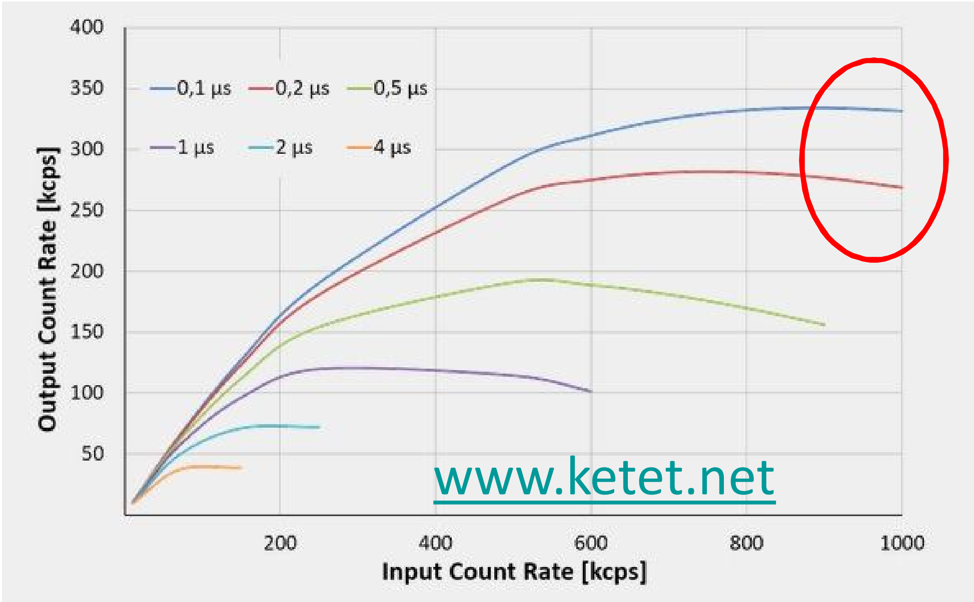

Larger area SDD's do not lead necessarily to proportional increase of detected intensities in high count rate applications due to increased dead time. Coupling detector operation with suitable signal processing unit is a key elements for fully exploiting larger areas SDD's

Energy Response of X-Ray Detectors

Fe-55 spectrum

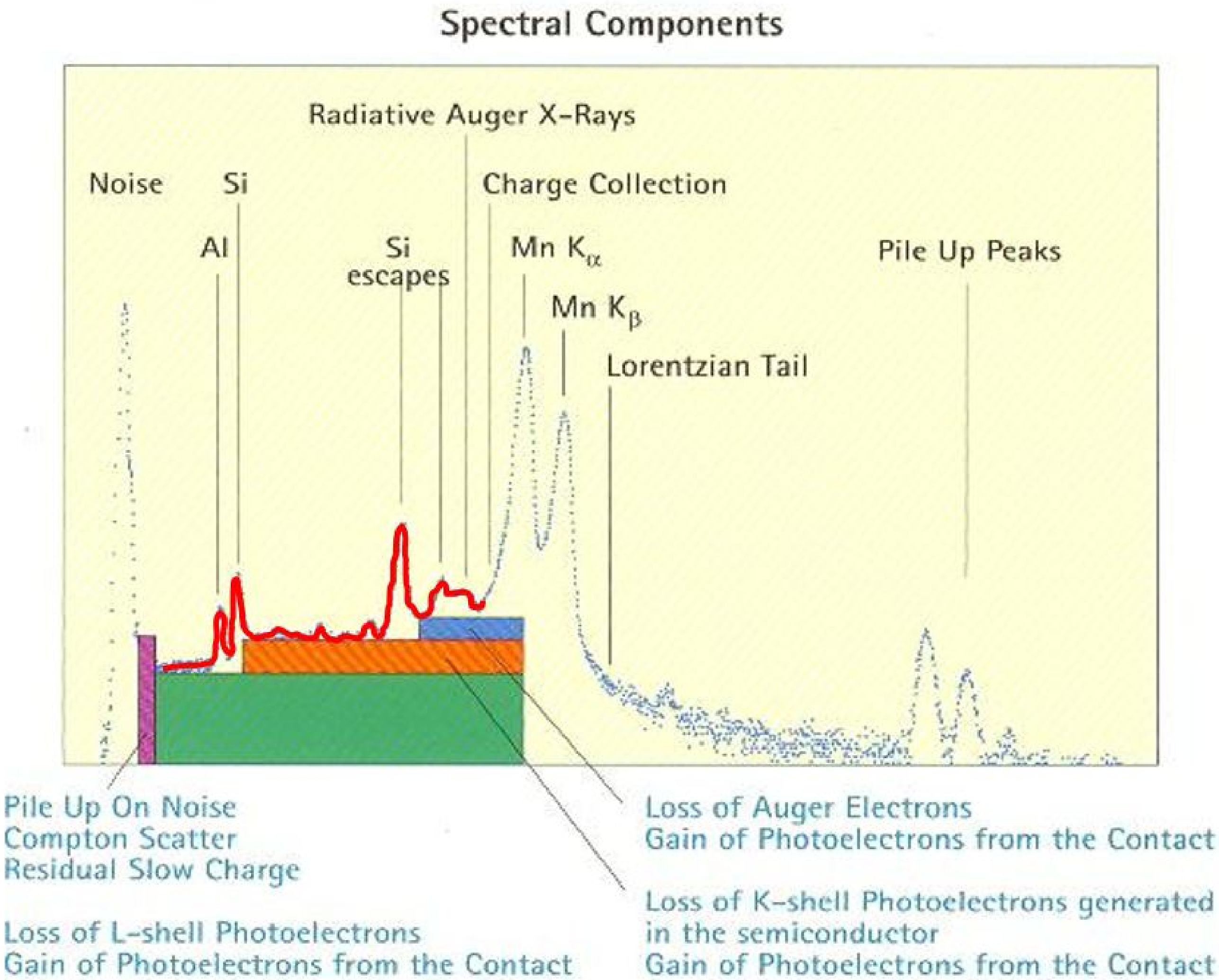

Energy Response of X-Ray Detectors

Background generated in XRF spectrum

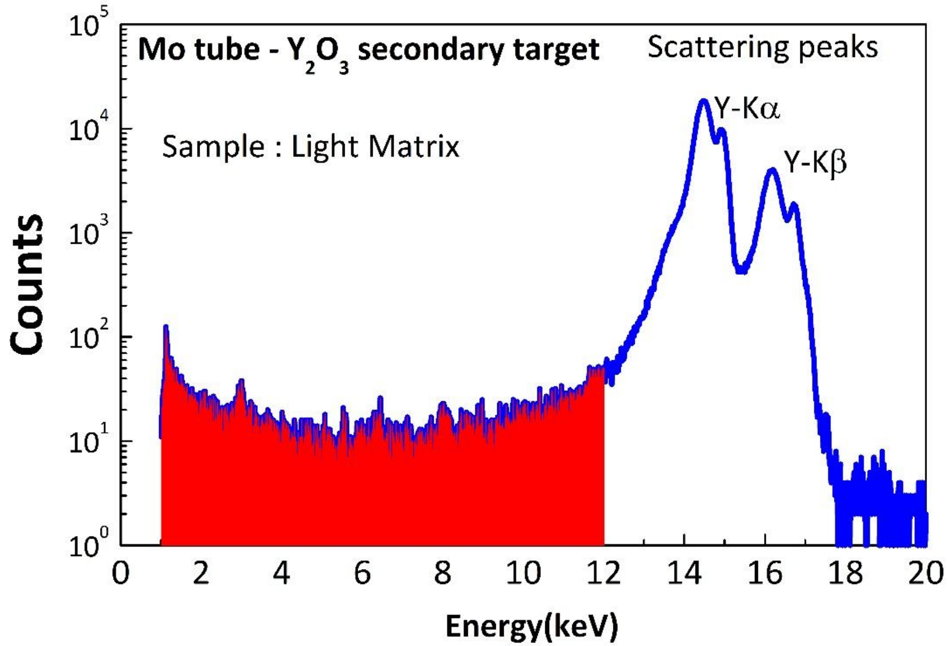

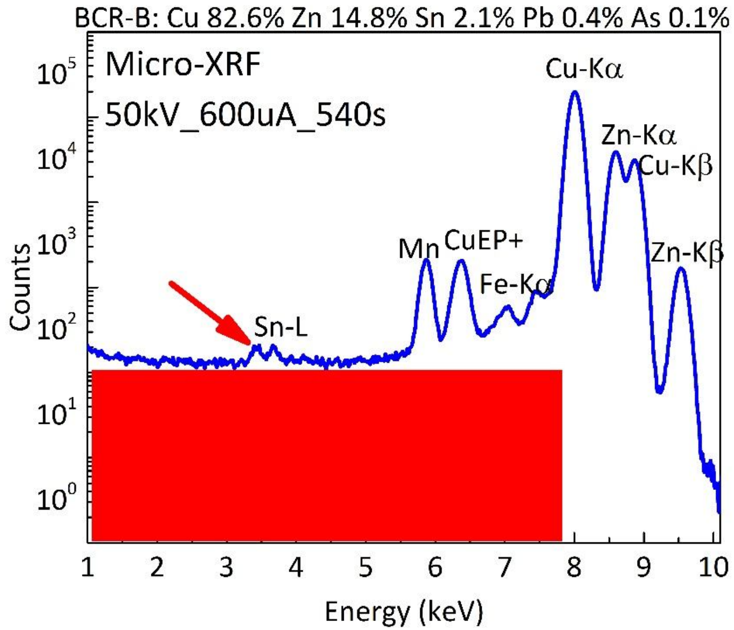

Background in light matrices:
- Scattered Source radiation

Metallic matrices:
- Fluorescent peaks of the major alloy elements

X-ray Detection in Full Field Geometry

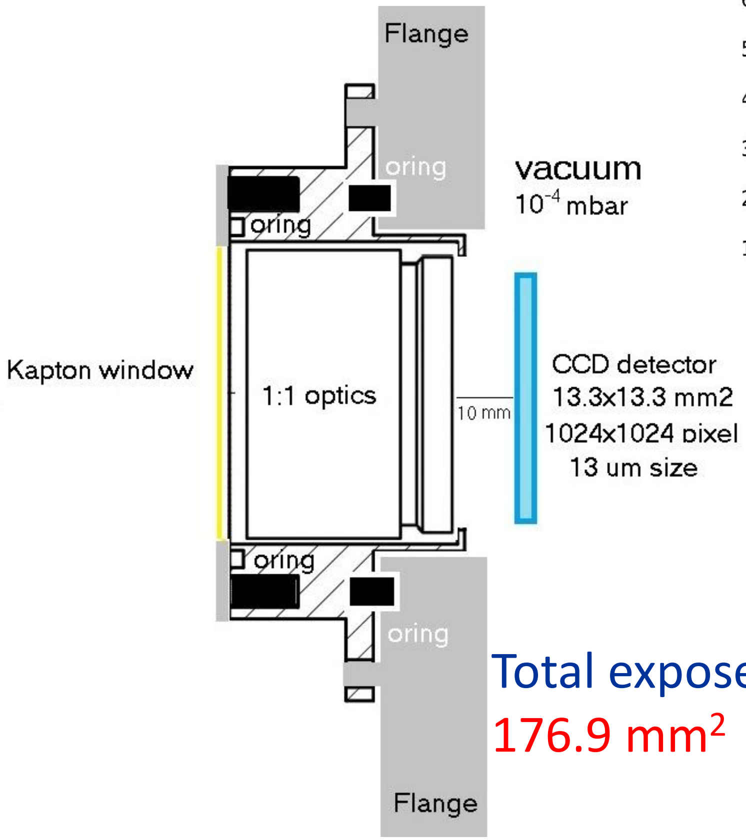

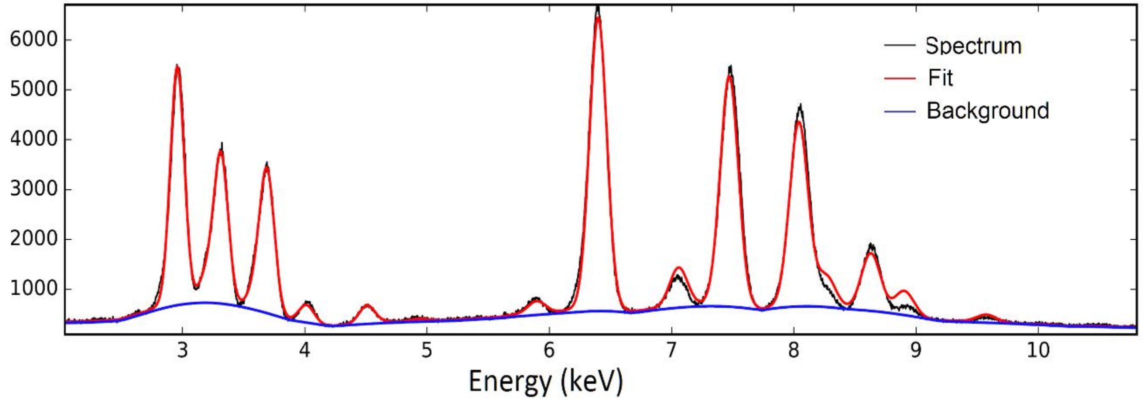

FWHM<155eV@MnKα

Total exposed area:
176.9 mm^2

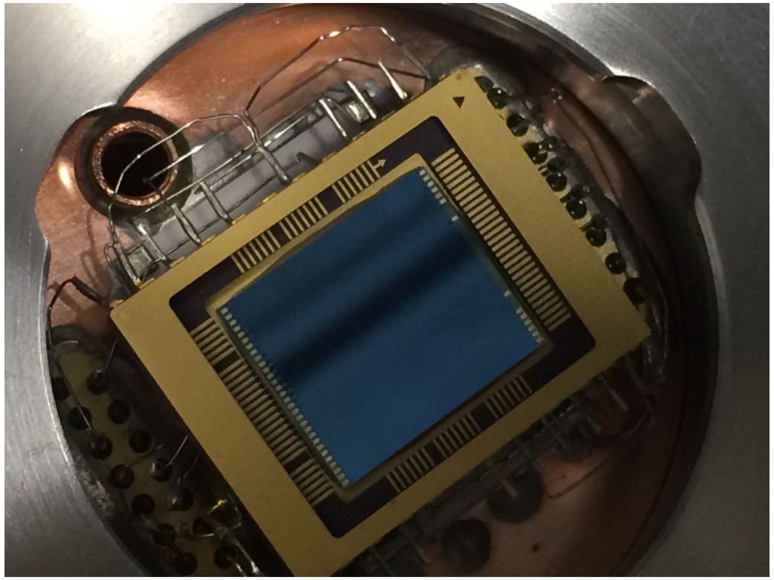

The CCD sensor is composed of 1024 × 1024 pixels with 13μm lateral size and 40 μm thickness, readout speed of the CCD can be programmed from 50kHz to 5 MHz

F.P. Romano et. al. Anal. Chem. 2016, 88, 9873−9880

XRF Analytical Sensitivity

LoD: Limit of Detection

$$(LoD)_i \approx 3 \cdot c_i \cdot \frac{\sigma_i}{N_i}$$ (95%) CL

$$\sigma_i \approx \sqrt{N_B}$$

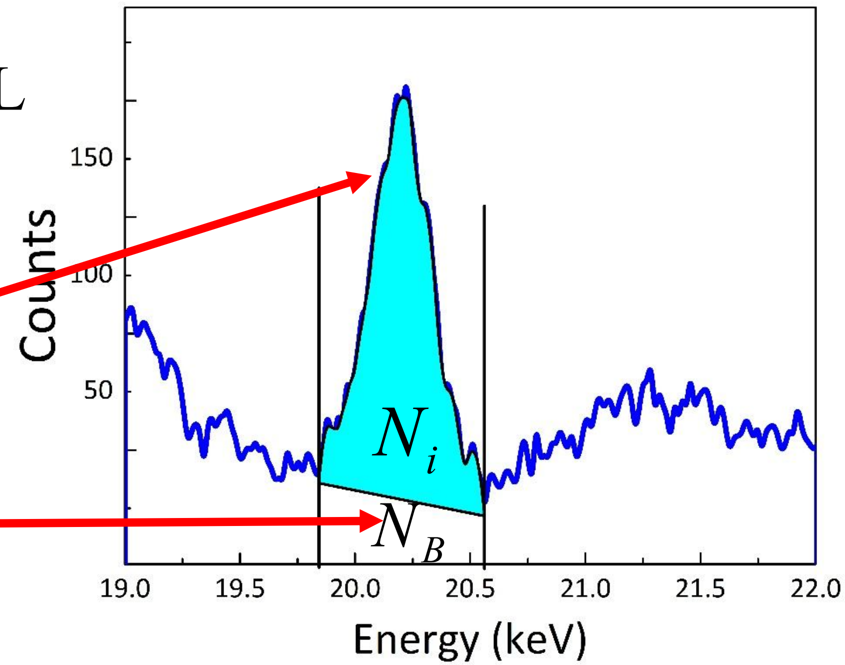

I_i Fluorescent intensity (cps)

I_B Background intensity (cps)

c_i Analyte concentration

$$(LoD)_i \approx 3 \cdot \frac{\sqrt{I_B / t}}{(I_i / c_i)} \propto \frac{\sqrt{t}}{t}$$

$$LoQ \approx 3.3 \cdot LoD$$

Figures of merit: Tube based MA-XRF

M. Alfeld et. al., JAAS 2011

A	B	C
Kevex Microfocus PXS4-613	MOXTEK 50 kV "Magnum"	XOS X-beam Powerflux
Mo	Rh	Mo
Inspector CSERF (Canberra)	DXP-XMAP (XIA)	DXP-XMAP (XIA)
10 × 10	60 × 25 (hor. × vert.)	60 × 25 (hor. × vert.)
1	4	4

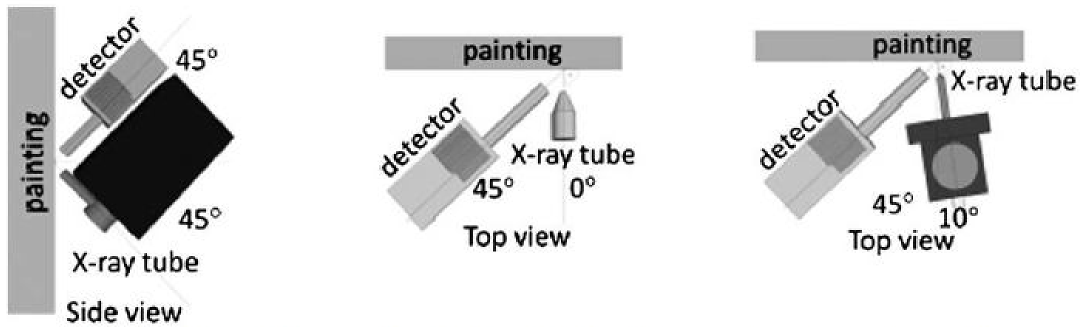

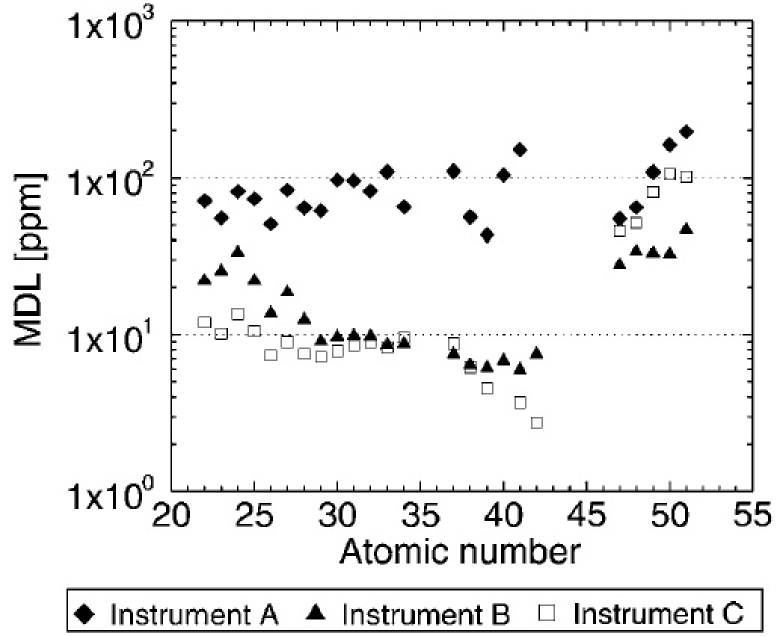

F.P. Romano et. al. JAAS 2017

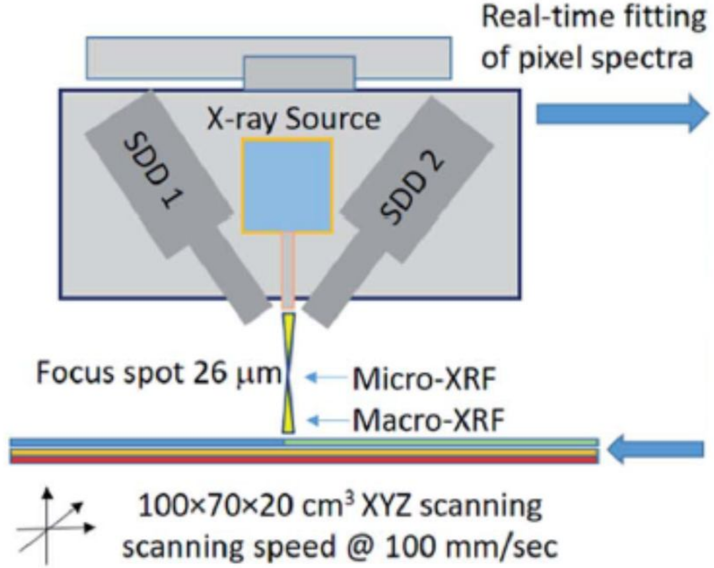

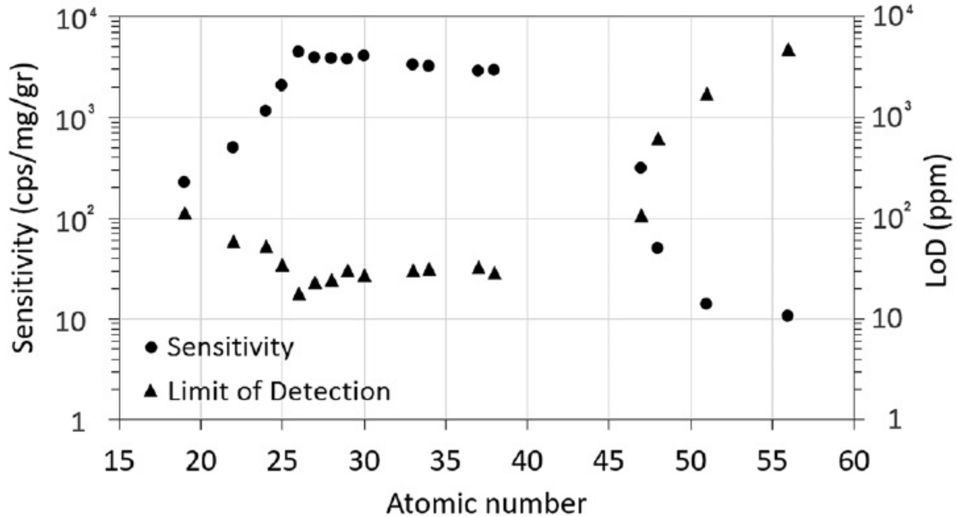

Figures of merit: Synchrotron based MA-XRF

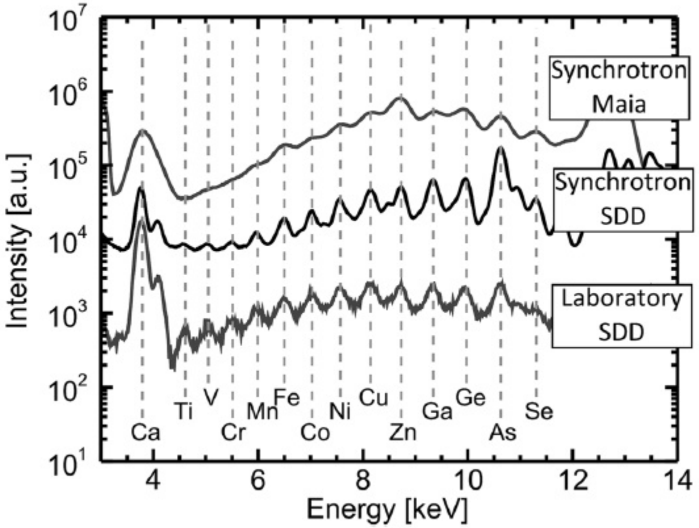

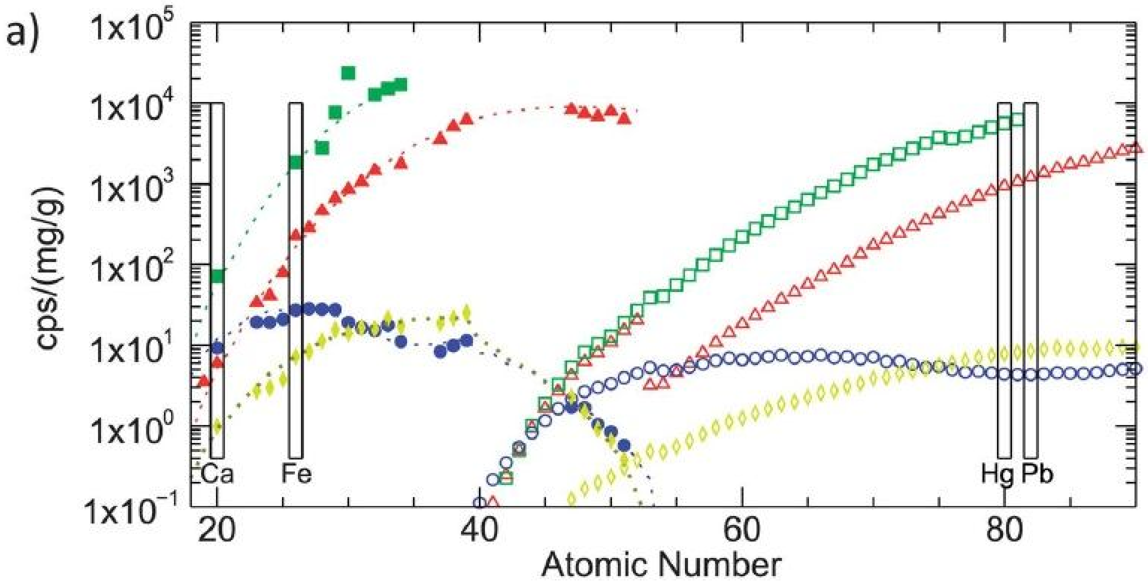

M. Alfeld et al. JAAS, 2013, 20, 40

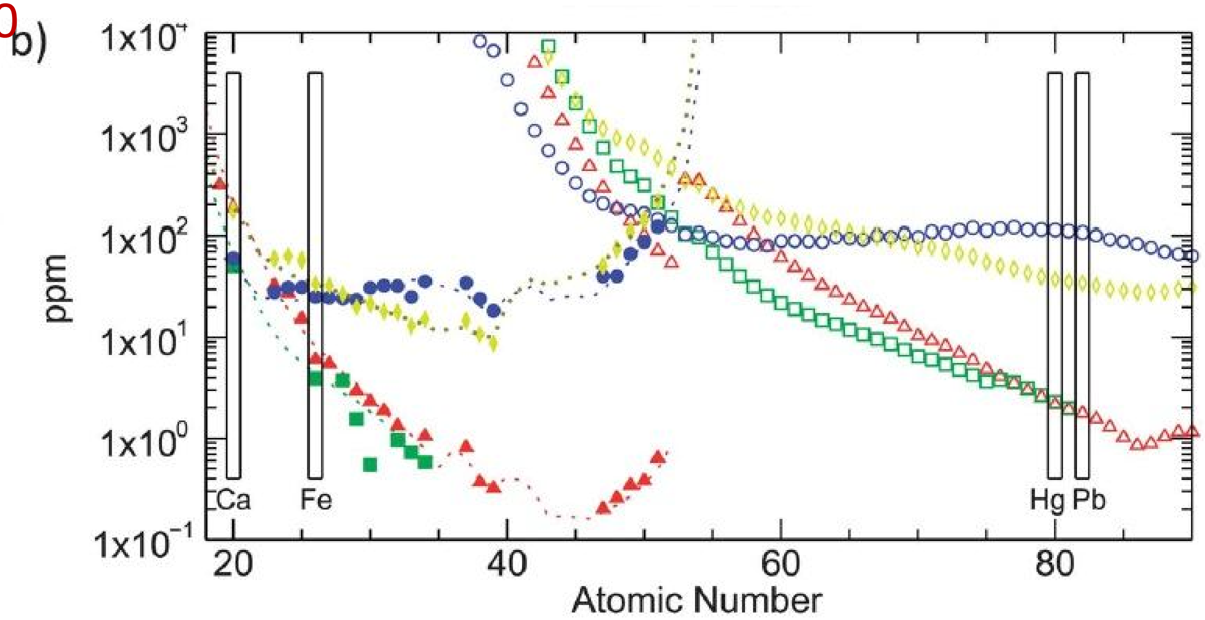

- ▲ K−Lines, 32.0 keV (Syn.), SDD
- ■ K−Lines, 12.7 keV (Syn.), Maia
- ● K−Lines, X-ray tube, Polycapillary
- ♦ K−Lines, X-ray tube, Collimator
- △ L−Lines, 32.0 keV (Syn.), SDD
- □ L−Lines, 12.7 keV (Syn.), Maia
- ○ L−Lines, X-ray tube, Polycapillary
- ◊ L−Lines, X-ray tube, Collimator

XRF Information depth

Material	X-ray line	D (μm)
Bronze **95% Cu, 5% Sn**	**Cu-Kα**	**10**
	Sn-Kα	32
Gold 95% Au, 4.5 % Ag, 0.5% Cu	Cu-Kα	1.4
	Au-Lα	2
	Ag-Kα	5
Egyptian Blue 20% + 80% binder	Cu-Kα	270
	Ca-Kα	37
	Si-Kα	6

The information depth depends on:

- the sample matrix composition
- analyte energy
- incident beam energy (spectrum)
- geometry (incident/outgoing angles)

Critical thickness

$$D = \frac{1}{\rho \cdot \mu_T(E_i)}$$

$$\mu_T(E_o, E_i) \equiv \mu_s(E_o)/\sin\vartheta_1 + \mu_s(E_i)/\sin\vartheta_2$$

XRF Information depth

80%Pb+20% alpha-linolenic acid as organic medium absorbing 90% of the emitted radiation

Material	X-ray
Bronze 95% Cu, 5% Sn	
Gold 95% Au, 4.5 % Ag 0.5% Cu	
Egyptian Blue 20% + 80% binde	

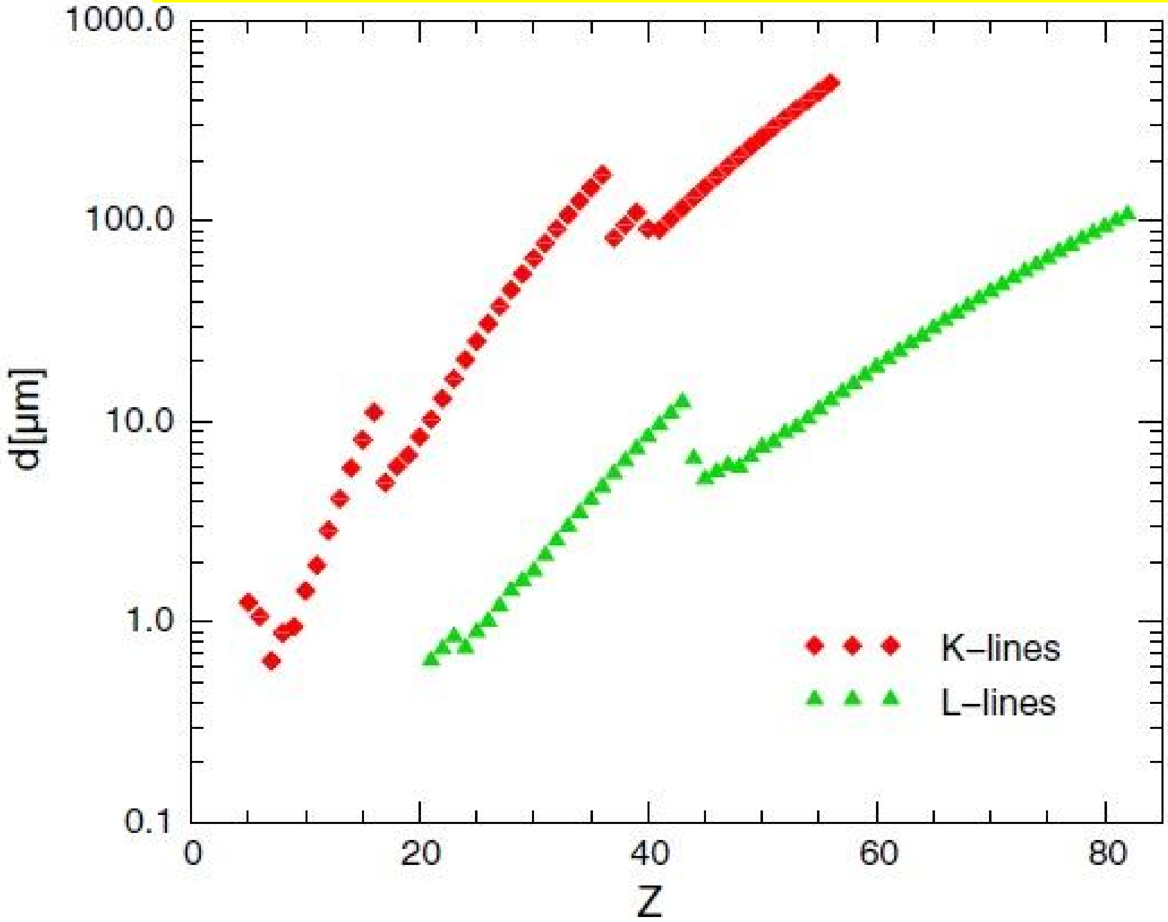

ends

sition

ing

M. Alfeld, J.A.C. Broekaert , SAB 88 (2013) 211

Critical thickr

$$D = \frac{1}{\rho \cdot \mu_T(E_i)}$$

$$\mu_T(E_o, E_i) = \mu_s(E_o)/\sin\theta_1 + \mu_s(E_i)/\sin\theta_2$$

Overview - Conclusions

- ✓ The advanced MA-XRF imaging capabilities are supported by the improved performance of X-ray detectors, digital signal processors, and X-ray focusing devices, but also by the availability of brilliant sources and fast spectrum analysis packages
- ✓ The underlying physics in MAXRF imaging are common amongst the different XRF variants. However, the integration of multiple and variant geometry detection systems helps to acquire XRF signals which incorporate improved information regarding the sample morphology and even in-depth elemental distributions
- ✓ State of the art MAXRF spectrometers achieve remarkable figures, almost 100ppm/1sec LoDs for the optimum detected elements
- ✓ Precise quantification is hampered by the need to characterize optical components, however elemental associations can be revealed by statistical treatment of the generated large datasets

Thank you for your attention!!

Acknowledgements

Paolo Romano, Claudia Caliri, Vasilike Kantarelou and Ch. Zarkadas